SCF/SCFR signaling plays an important role in the early morphogenesis and neurogenesis of human embryonic neural retina

Yu Gong,[1,2] Xiangyu He,[2] Qiyou Li,[1,2] Juncai He,[1,2] Baishijiao Bian,[1,2] Yijian Li,[1,2] Linlin Ge,[1,2] Yuxiao Zeng,[1,2] Haiwei Xu,[1,2,‡] and Zheng Qin Yin[1,2, ‡]

[1] Southwest Hospital/ Southwest Eye Hospital, Third Military Medical University (Army Medical University), Chongqing, P.R. China

[2] Key Lab of Visual Damage and Regeneration & Restoration of Chongqing, Chongqing, P.R. China

‡Authors for correspondence : xuhaiwei@tmmu.edu.cn (Haiwei Xu), qinzyin@aliyun.com (Zheng Qin Yin)

Summary statement:We show an unreported role of SCF/SCFR signaling in the early embryonic development of human eye.

Abstract:

The stem cell factor receptor (SCFR) has been demonstrated to be expressed in the neural retina of mice, rat, and human for decades. Previous reports indicate that SCFR correlates with glia differentiation of late retinal progenitor cells (RPCs), retinal vasculogenesis, and homeostasis of the blood-retinal barrier. However, the role of SCF/SCFR signaling in the growth and development of the neural retina (NR), especially in the early embryonic stage, remains poorly understood. Here we show that the SCF/SCFR signaling orchestrates invagination of the human embryonic stem cell (hESC)-derived NR via regulation of cell cycle progression, cytoskeleton dynamic, and apical constriction of RPCs in the ciliary marginal zone (CMZ). Furthermore, activation of SCF/SCFR signaling promotes neurogenesis in the central-most NR via accelerating the migration of immature ganglion cells and repressing apoptosis. Our study reveals an unreported role of SCF/SCFR signaling in controlling ciliary marginal cellular behaviors during early morphogenesis and neurogenesis of the human embryonic NR, providing a new potential therapeutic target for human congenital eye diseases such as anophthalmia, microphthalmia, and congenital high myopia.

Introduction

The eye is the most important sensory organ that receives and transduces light signals to the visual cortex. Functional visual organs require specific morphological structures and appropriate size control. During early embryogenesis, the retinal neuroepithelium, which arises from the retinal anlage, evaginates laterally from the diencephalic wall to form an optic vesicle (OV). The distal portion of the OV then invaginates to form a cup-like structure, the optic cup (OC), with the neural retina (NR) and the retinal pigment epithelium (RPE) being the inner and outer walls, respectively. Any abnormalities of these sequential steps of OC morphogenesis leads to severe eye diseases such as anophthalmia, microphthalmia, and coloboma (Heavner and Pevny, 2012).

Invagination of the NR is critical for OC formation (Fuhrmann, 2010). Recent studies of the self-organized OC from human embryonic stem cells (hESCs) suggested that OC formation is a spontaneous process that consists of three consecutive local processes (relaxation of the NR, apical constriction of the hinge region, and tangential expansion) (Eiraku et al., 2012). Adjacent to the hinge region where invagination of the NR occurs is the ciliary marginal zone (CMZ), which serves as a stem cell pool for de novo retinal neurogenesis during vertebrate eye development (Belanger et al., 2017;Fischer et al., 2013;Kuwahara et al., 2015).

The stem cell factor (SCF) receptor SCFR, also known as KIT or CD117, is a 145 kDa transmembrane tyrosine kinase encoded by the SCFR proto-oncogene and is essential for gametogenesis, hematopoiesis, and melanogenesis (Lennartsson and Ronnstrand, 2012). Its specific inhibitors, such as imatinib, have been well applied in the treatment of chronic myelogenous leukemia (CML) and acute lymphocytic leukemia (AML) for decades. SCFR and SCF are expressed in both peripheral nervous system (PNS) and central nervous system (CNS) and are involved in the survival, proliferation, differentiation, and maturation of neural stem cells (NSCs) (Das et al., 2005a). Das et al. reported that SCFR expression is upregulated in ciliary epithelium (CE) NSCs *in vitro*, suggesting that signaling mediated by SCFR may represent a mechanism utilized by stem cells in the optic neuroepithelium (Das et al., 2005b). In addition, SCFR is thought to be involved in the organization of the neural tube and the brain (Keshet et al., 1991). However, the role of SCF/SCFR signaling in the growth and development of the NR, especially in the early embryonic stage, remains poorly understood.

The majority of previous reports about OC morphogenesis are based on researches on the mouse retina. Our understanding of human embryonic retina development is limited to ethical constraints. Recently, OCs were self-organized from both the ESCs and induced pluripotent stem cells (iPSCs) via a stepwise method, which opened the door to achieving high fidelity in simulating human retina development and served as an ideal

disease model *in vitro* (Eiraku et al., 2011;Kuwahara et al., 2015;Nakano et al., 2012;Pasca, 2018;Rossi et al., 2018).

Here, we utilized the self-organized optic cups from hESCs to investigate the biological function of SCF/SCFR signaling during early development of the human embryonic NR. It was demonstrated that SCF/SCFR signaling facilitated human NR invagination by accelerating cell cycle progression of retinal progenitor cells (RPCs), regulating cytoskeleton dynamics and enhancing the apical constriction in the CMZ. In addition, we found that the activation of SCF/SCFR signaling produced a premature neuro-retina in the central NR (cNR) by promoting the migration of immature ganglion cells and repressing cellular apoptosis.

RESULTS

Generation of hESC-derived OC with the CMZ

To recapitulate human embryonic retinal development with the least amount of extrinsic factors, we utilized the NR selective protocol previously described by Kuwahara et al. (Kuwahara et al., 2015). Dissociated hESCs (Line H1 WA01) were first reaggregated in a low-cell-adhesion V-bottom 96-well plate (10,000 cells/well). Embryonic bodies were induced by transient early treatment of BMP4 at D6 in suspended culture and more than 4.16% further developed into a patterned layered retinal morphology with pigment accumulation by D24 (Fig. 1A). The qRT-PCR analysis showed the loss of pluripotency (downregulation of OCT4) and specification of the eye field (upregulation of Rax, Pax6, and LHX2) of hESC aggregates after 24 days of differentiation (Fig. S1A). Retinal organoids acquiring a two-domain morphology consisting of the NR and RPE at D24 were collected and depicted as the OC (Fig. 1B). The eye field transcription factor Rax and NR progenitor markers Chx10 and Sox2 were restricted in the apical layer of the thick NR portion, while the RPE progenitor marker MITF was restricted to the thin RPE portion (Fig. 1C, D, E). Pax6 was expressed throughout the NR and across the NR-RPE junction, whereas the pluripotent marker SSEA4 was negative in the OC (Fig. 1D, E). The majority of cells in the OC were positive for the mitotic marker Ki67 (Fig. S1B,C). In the NR region, Ki67 was mainly located in the Chx10^{+} RPCs on the apical side of NR (Fig. S1L), while the basal side was occupied by Nestin-positive radial glia, such as neural progenitor cells (Fig. S1J,K). The CMZ emerged as a tapering region directly adjacent to the pigment-accumulated RPE domain (Fig. 1F,G,H). In contrast to the cNR region, which comprised a dense apical layer and a loose basal layer, there was only one compact cell layer in the tapering CMZ (Fig. S1D, E). Ki67^{+} cells were sparsely distributed in the distal tip of the CMZ but became dense in the proximal subdomain (Fig. S1F). The expression of P27kip1, the CDK inhibitor that positively controls cell cycle exit (Dyer and Cepko, 2001), was

absent in the CMZ (Fig. S1G). The specific molecular marker of the ciliary margin SSEA1 (Koso et al., 2008) was expressed in the Chx10^{+} domain (Fig. 1I,S1H), while the pigmented ciliary epithelium marker AQP1 (Yamaguchi et al., 2006) was expressed only in the MITF[+] domain adjacent to the junction (Fig. S1I). These data demonstrated a well-established human OC derived from hESCs, which was characterized by classical morphology, including the CMZ.

SCFR is strongly expressed and spatiotemporally confined in the CMZ of the human OC

SCFR is distributed in multiple systems of vertebrate organisms, but limited information is available regarding its expression in the CNS (Lennartsson and Ronnstrand, 2012). To determine the expression pattern of SCFR during development of the human retina, we detected the SCFR signal by immunostaining OCs at different stages. During the induction of human OC, SCFR first emerged at the outer portion of embryonic bodies at D6, gradually enriched at the epithelium-like cells at D12 (Fig.S2b), and robustly located at the optic vesicle at D18 (Fig.S2A~C). At D24, the primary time of OC formation (Nakano et al., 2012), SCFR was specifically expressed in the whole NR, with strong labeling at the NR-RPE border, but completely negative in the RPE (Fig. 2A, B;). The SCFR[+] region of the NR could be segregated into two parts: a central Sox2^{+}/SCFR[-dim] domain and a peripheral Sox2^{-}/SCFR[-strong] domain (Fig. 2A; S6C), which was characterized as the tapering monolayered CMZ (Belanger et al., 2017). The gray intensity of SCFR signal in the CMZ is almost 1.5~2.5-fold higher than that in the nonmarginal NR at each development time point (Fig. 2C), indicating that SCFR is strongly expressed in the CMZ in a spatially dynamic pattern. At D31 (D24+1W), the expression of SCFR remained strong in the CMZ but gradually reduced in the nonmarginal NR. At D38 (D24+2W), SCFR only remained at the most distal tip of the CMZ or the NR-RPE junction. By approximately D45 (D24+3W), the whole OC tissue had lost SCFR expression, and only part of nonretinal tissue around the OC maintained a relatively low expression of SCFR (Fig. 2E). Consistently, the mRNA level of SCFR determined by qRT-PCR analysis also showed a continuous decrease depending on the developmental stage of OC from D24 to D45 (Fig. 2D). Thus, SCFR is strongly expressed and confined in the CMZ of hESCs-derived OCs in a spatiotemporal manner (Fig. 2F). On the other hand, SCF, the ligand of SCFR, was not robustly expressed in the basal side of the central SCFR positive NR until D18 when the original optic vesicle formed(Fig. S2A~E). Consistently, the phosphorylation of SCFR emerged at the basal side of the cNR as well as remained at a relatively low level in the CMZ (Fig. S2H,K). Taken together, these results demonstrated that SCF/SCFR signaling plays a role in the early development of human NR.

Activation of SCF/SCFR signaling facilitates NR invagination and increases axial length

SCF/SCFR signaling plays important roles in cell migration, proliferation, and differentiation in the CNS (Matsui et al., 1990). The strong expression of SCFR in the CMZ raised the question of what role it may play in the development of the human OC. To address this issue, we administered SCF, the ligand of SCFR, and its inhibitor isck03 to the 3D developing OC from D24 to D30, at which time the primary OC is formed (Fig. 3A). In the control condition, the NR-RPE angles were mainly obtuse ($104.0\pm4.3°$) at D24 when the two-domain NR-RPE retinal organoid primarily formed. As development proceeded to D38, majority of the NR-RPE angle gradually became acute ($58.3\pm6.2°$). The perpendicular angle ($90.8\pm4.1°$) was somehow an intermediate state around D31 (Fig.3B,C). Notably, the variability of the NR-RPE angle between D24 and D30 remarkably increased after SCF administration, suggesting that SCF/SCFR signaling might positively participate in invagination of the NR. However, it shows that there is a balance, since isck03 seems to reduce the angle but not completely (Fig. 3D), and the presence of SCF has the opposite effect. In addition, we observed that the CMZ began to transform into an elongated and wedge-like morphology from the third day of SCF administration, while the CMZ of the control group remained short and column-like. On the 6th day of SCF treatment, the CMZ had further elongated and exhibited a slim, spindle-like, sharp tapering shape (Fig. 3E). It was noteworthy that the axial length of the SCF-treated OC was even 100 μm longer than that of the control group. Moreover, the SCF-treated CMZ became significantly longer and thinner (Fig. 3G,H), suggesting that the expansion of CMZ may contribute to overgrowth of the axial length. Moreover, we found the extended expression of SSEA1 in the SCF-treated CMZ and loss of SSEA1 expression in the isck03-treated CMZ (Fig. S3A~C). Theses results indicated that SCF/SCFR signaling is involved in the development of CMZ.

SCF/SCFR signaling orchestrates the cell cycle progression in the CMZ

Cell proliferation is the key internal driving force during invagination of the NR (Sasai, 2013). Hence, we sought to investigate the influence of SCF/SCFR signaling on the proliferation of CMZ-RPCs. To this end, we performed a pulse-labeling experiment using nucleotide analogues BrdU (Fig. 4A). The cell cycle length of the RPCs in the CMZ is less than 24 hours (Fig. S4A,B,C) and most of the Ki67+ cells in the CMZ exited the cell cycle after one round of cell cycle within 24 hours(Fig.S4G). Moreover, the entrance or exit of the cell cycle seems to be independent of SCF/SCFR signaling as neither SCF nor isck03 treatment produced a significant difference in the proportion of BrdU+/Ki67+ cells in the BrdU+ cells and Ki67+ cells in the total cells 24 hours after BrdU

incorporation (Fig.S4H,I). However, the proportion of BrdU$^+$/Ki67$^+$ cells in the CMZ were markedly reduced by SCF treatment and increased when the blocker of SCFR isck03 was administrated at the intermediate stage (12 hours after BrdU incorporation) (Fig.S4J). This clued that SCF may shorten the cell cycle length of RPCs and inhibition of SCFR prolonged the cell cycle (note that it was still within 24 hours). To verify this result, OCs were incubated with BrdU in the presence of SCF or isck03 for 12 hours (Fig. 4C,D). Compared with the control group, the accumulation of BrdU in the CMZ was greatly enhanced by SCF treatment. As a contrast, the isck03 did not perturb the BrdU accumulation of RPCs (Fig. 4 D, F). To further confirm this result, we performed a BrdU dilution experiment(Fig. 4A). The 24-hour exposure of 3D OCs to BrdU heavily labeled the progenitor cells in the CMZ (Fig. 4B, E). As shown in the control group, BrdU$^+$ cells in the CMZ were diluted after an additional 72 hours (+96 h), and 21.1±1.8% of CMZ-RPCs remained BrdU-positive. Surprisingly, BrdU$^+$ cells in the CMZ following SCF treatment were largely diluted, and fewer CMZ-RPCs remained BrdU-positive. In addition, the treatment of isck03, the specific inhibitor of SCFR, reversed this accelerated dilution phenomenon, leaving approximately 41.4% BrdU$^+$ cells in the CMZ (Fig. 4B, E). As no cell apoptosis was observed in the CMZ(Fig 6S), the more BrdU diluted, the more cell cycles the cells have gone through, which comfirmed the accelerated cell cycling by SCF. Taken together, these results demonstrated that SCF/SCFR signaling orchestrates the cell cycle progression of RPCs, thus modulates the cell dynamics in the CMZ and further contributes to the morphogenesis of the NR.

Given that the central-peripheral (horizontal) orientation of cell division is highly correlated with the symmetric division in the developing retina (Agathocleous and Harris, 2009;Cayouette and Raff, 2003;Das et al., 2003;Zhong and Chia, 2008;Zigman et al., 2005), the tangentially elongated CMZ after SCF treatment suggested that SCF/SCFR signaling might expand the stem cell pool via promotion of symmetric division of CMZ-RPCs. To further reveal the effect of SCF/SCFR signaling on the mode of CMZ-RPC division, we analyzed the spindle orientation of CMZ-RPCs by p-vimentin and Ki67 labeling (Fig. 4G). We observed the mixed orientation of division in the CMZ and the cNR. In the control group, we observed mainly horizontal orientation (47%) with some oblique (28%) and vertical (25%) orientation, indicating a robust symmetric division in the CMZ (Fig. 4H). However, in the cNR, 38% of cell divisions were horizontal, 26% were oblique, and 36% were vertical (Fig. 4I), suggesting an increased tendency in the asymmetric division in the cNR, as described in previous reports (Harris and Perron, 1998;Larsen et al., 2009). Nevertheless, the perturbation of SCF/SCFR signaling did not alter the pattern of spindle orientation in both the CMZ and the cNR (Fig. 4H,I). These results indicated that the SCF/SCFR signaling orchestrates the cell cycle progression in the CMZ to produce a tangentially biased driving force within the internal CMZ, contributing to invagination of NR and the increased axial length.

SCF/SCFR signaling regulates cytoskeleton dynamics and apical constriction of the CMZ

The accelerated invagination of NR prompted us to answer the question of whether SCF/SCFR signaling regulates the mechanical dynamics of NR to facilitate deformation. To this end, we analyzed the cytoskeleton dynamics of NR by detecting F-actin assembly/disassembly by phalloidin staining because apical F-actin regulates the exocytosis of cells and alters the construction of extracellular matrix to change the tissue rigidity during rapid expansion of the apical surface (Wang et al., 2013). Cellular cytoskeletons of apical cells lost their continuous expression in the nonmarginal NR after SCF treatment and disassembled in the CMZ compared with the control group, which exhibited a more continuous F-actin construction (Fig. 5A,B). Disassembly of F-actin made the CMZ tissue more flexible and facilitated folding toward the RPE in this region, contributing to morphogenesis of the optic cup according to a previous atomic force microscopy analysis of the 3D neural retina (Eiraku et al., 2011). However, the treatment of isck03 kept the integrity of F-actin both in the CMZ and central NR (Fig. 5C), demonstrating an active role of SCFR in the cytoskeleton dynamic of NR. To investigate the driving force facilitating the invagination of the NR, we further examined actomyosin activity of the RPE-NR junction by immunostaining of phosphorylated myosin light chain 2 (pMLC) because invagination of the NR depends strongly on the fold direction, as evagination will occur if the NR folds in the opposite direction. Surprisingly, pMLC activity was significantly stronger after SCF treatment than in the control group in the apical CMZ but remained unchanged in the nonmarginal NR and relatively weak in the isck03 treatment group (Fig. 5D, E, F). This result strongly indicates that SCF/SCFR signaling robustly enhances the activity of pMLC in the apical CMZ, which pulls the NR toward the RPE, thus accelerating the formation of an acute angle between the RPE and the apical surface of the NR. As inhibition of myosin activity may disrupt polarity of the apically convex Chx10$^+$ epithelium of 3D retinal organoids (Lowe et al., 2016), we performed ZO-1 staining to assess the apical-basal polarity of the NR after SCF treatment. Consistent with the control group, ZO-1 was continuously located on the surface of the outer cell layer of the NR after SCF and isck03 treatment, indicating that SCF/SCFR signaling does not affect NR polarity (Fig. 5G, H, I). Thus, SCF/SCFR signaling regulates cytoskeleton dynamics and apical constriction of the CMZ to facilitate invagination of the NR, thereby accelerating formation of an acute angle between the RPE and the apical NR.

Activation of SCF/SCFR signaling promotes the migration of immature ganglion cells, represses cellular apoptosis, and produces a premature neuro-retina

In the human fetal eye, the differentiation of ganglion cells and cone photoreceptor cells begins in the central-most NR, eventually gives rise to the fovea (O'Brien et al., 2003). We found that the OCs of the SCF treatment group usually had a much thicker compacted inner cell layer in the central-most NR than that in the control and isck03 group (Fig. 6A,B,I,J). The thickened inner cell layers of the NR were contained numerous Pax6^{+}, Brn3b^{+} and p27kip1^{+} cells (Fig. 6C~H), which mark naïve ganglion cells, the first-born NR cell lineage, located in the inner cell layers (Cayouette et al., 2006). This finding led us to investigate the migration of naïve ganglion cells as the apical-basal migration if the essential process of neuron maturity in the CNS(Xu et al., 2015). Tuj1^{+} ganglion cells emerged in the nonmarginal NR and migrated from the apical region toward the basal side along the processes of Nestin[+] radial glia-like cells (Fig. S1B,J,K). Surprisingly, significantly more Tuj1^{+} ganglion cells migrated in the outer cell layer of the central-most NR following SCF treatment (Fig. 6K,M~R). However, this phenomenon was defective in the isck03-treated NR(Fig. 6K,Q,R). Moreover, cleaved-caspase3^{+} apoptotic cells were dramatically decreased in the SCF-treated NR and increased in the isck03-treated group (Fig. 6L,S~U). The enhanced migration of immature ganglion cells and the repressed apoptosis by SCF treatment together suggest that SCF/SCFR signaling may also play a role in the development of the ganglion cell layer and the formation of the retinal neural circuit. To further explore whether SCF/SCFR signaling is involved in the production of the presence progenitors, we further analyzed multiple committed retinal progenitor/precursor cells marker such as Islet1(ganglion cell progenitor/precursor cell), Crx (photoreceptor progenitor/precursor cell), Calretinin (interneuron progenitor/precursor cell), and CRALBP (Müller progenitor/precursor cell) in the central NR. During vertebrate retina development, six types of neuron and one type of glia are generated in a conserved order: ganglion cells generated first, and rods, bipolar cells and Müller glia produced last (Livesey and Cepko, 2001). These committed progenitor cells were sparsely generated by the retinal organoid at D30 (Fig.S5A,D,G,J,M,N). The inducement of SCF promoted the genesis of Islet1^{+}, Calretinin[+], and CRALBP[+] progenitor/precursor cells but did not affect the production of Crx[+] photoreceptor progenitor cells (Fig.S5B,E,H,K,M,N). Similarly, the treatment of isck03 remarkedly increased the amount and proportion of all the committed progenitor/precursor cells (Fig.S5C,F,I,L,M,N). This result indicated that the imbalance of the SCF/SCFR signaling disturbed the early development of NR and result in a premature neuro-retina. It is worth mentioning that the mechanism beneath the pre-mature effect of SCF and isck03 on the NR development might be complex since there was a differential production bias in the photoreceptor, interneuron, and neuroglia progenitor/precursor cells (Fig.S5M,N). As for

the actively proliferating cells in the CMZ, they were not directed to produce terminally differentiated postmitotic cells (Kuwahara et al., 2015). Similarly, we did not observe any positive signal of these committed presence progenitor/precursor cells in our experiment. To summarize, all the above data supported that the SCF/SCFR plays an important role in the early neurogenesis of NR.

DISCUSSION

Organogenesis of the vertebrate eye is a multistep process that starts with the formation of optic vesicles followed by invagination of the distal optic vesicle resulting in morphogenesis of the OC. Many congenital eye disorders, including anophthalmia, microphthalmia, coloboma, and retinal dysplasia, stem from disruptions in the formation of the embryonic eye (Fuhrmann, 2010). How the unique shape of the optic cup is determined remains to be an intriguing topic for many decades. Several extrinsic and intrinsic determinants such as fibroblast growth factors (FGFs), bone morphogenetic proteins (BMPs), retinoic acid (RA) have been identified to contribute to the specification and morphogenesis of the OC (Chen et al., 2013;Heermann et al., 2015;Picker and Brand, 2005;Valdivia et al., 2016). However, we still suffer from a huge lack of understanding about the mechanism of OC formation.

Expanding and integrating existing knowledge of the molecular and genetic machinery underlying retinal development is critical not only for elucidating normal developmental mechanisms but also for developing therapeutic interventions aimed at vision restoration (Bassett and Wallace, 2012). Determining the mechanism of OC morphogenesis in human fetal eyes, however, has been difficult due to stringent ethical limitations. In recent years, researchers have established several protocols to culture 3D retinal organoids from hESCs or iPSCs to obtain qualified laminated 3D retinal tissue and functional photoreceptors with outer segment (Eiraku et al., 2011;Nakano et al., 2012;Zhong et al., 2014). Combining these advanced techniques, we showed that SCF/SCFR signaling regulates proliferation, cytoskeleton assembly and apical constriction dynamics of RPCs in the CMZ of 3D human OCs, orchestrating invagination of NR and axial growth of OC. SCF/SCFR signaling also facilitated neurogenesis of the inner neuroblast cell layers in the central-most NR via promotion of immature ganglion cell migration and repressing cellular apoptosis, indicating that SCF/SCFR signaling plays a position-dependent role in the development of the human embryonic eye. Although SCF/SCFR signaling has been widely investigated in the tumorigenesis of acute myeloid leukemia (AML), melanoma, and gastrointestinal stromal tumors (GISTs), no reports have discussed the role of SCF/SCFR signaling in human embryonic eye development (Heinrich et al., 2002;Hirota et al., 1998;Woodman and Davies, 2010).

In this study, we showed that SCFR expression was expressed throughout the NR and gradually confined in the CMZ in a spatiotemporal manner (Fig. 2C). As for the human embryonic retina, SCFR was expressed both in the central NR and far peripheral NR and reached the highest level during 7th to 12th gestation week (Hasegawa et al., 2008;Zhou et al., 2015). The developmental stage of 3D retinal organoid may be 3~4 weeks earlier than human developing retina speculated by the expression time of Chx10 in the recent report on the integrated transcriptional analysis of the developing human retina(Fig. S2G)(Mellough and Bauer, 2019). The time-dependent difference and the defective periocular tissue in the retinal organoid may together contribute to the differential expression of SCFR between the retinal organoid and fetal eye. Moreover, this result is in contradiction with the expression pattern of SCFR in the mouse retina, in which SCFR is peaking at P0 and located in the central-most NR and expands toward the peripheral region except for the CMZ(Koso et al., 2007), indicating that the species difference cannot be ignored on the expression and function of SCFR.

The existence of niche-like ciliary marginal zone of vertebrate embryonic neuro-retina had identified in the mice and human retinal organoid recent years(Belanger et al., 2017;Kuwahara et al., 2015). Previous report proposed that the actively proliferating cells in the CMZ produce progenitors de novo by continuous cell division. Meanwhile, according to our data, the proportion of proliferating cells in the CMZ remained constant and no sign of apoptosis was observed in the CMZ at the early development stage of retinal organoid(Fig.S4I,K;Fig.6S). These results suggested that there might be a dynamical balance between the proliferation of stem cells and migration of progenitor cells in the CMZ, in which the SCF/SCFR signaling plays as an orchestrator. Moreover, heterogeneity of ciliary marginal cells is also a matter of intriguing problem that should be considered since we found the CMZ could actually be sub-divided into two part: a more periphery $Chx10^+/Sox2^-$ domain and a central $Chx10^+Sox2^+$ domain(Fig.S6C,D). This division pattern is reminiscent of the CMZ in the amphibian and fish retina which consist of the slowly dividing uncommitted stem cells in the far peripheral region, committed rapidly dividing progenitors in the central CMZ, and differentiated neurons at the central edge of the CMZ(Harris and Perron, 1998;Xue and Harris, 2012). On the other hand, the spindle oriental in the CMZ is mixed with horizontal, oblique, and vertical division mode(Fig.4G,H,I). This result further confirmed the cell heterogeneity in the CMZ. Our data revealed the function in regulating the cell cycle length of the SCF/SCFR signaling, which might contribute to the heterogeneity in the CMZ as disturbed cell cycle length of neural progenitors alter cell fate in the developing CNS(Pilaz et al., 2016). A conditional SCFR knock-out hESC cell line and detailedly distinguishment of cell types in the CMZ shall be needed in future research.

The invagination of NR is most crucial step in the morphogenesis of two wall-like optic cup. As the unique

anatomy region between the rigid RPE and relaxed NR, the CMZ is poorly discussed in this important morphological event. As we reported, the role of orchestrator in the cellular dynamic of CMZ endows the SCF/SCFR signaling with a power to drive the change of shape. On the other hand, SCF/SCFR signaling facilitates CMZ deformation by upregulating apical constriction and disassembled the cytoskeleton of apical cells. Sasai and his colleagues reported that pMLC activity completely disappeared in the 3D human OC(Nakano et al., 2012). However, in their model, a whole invaginated NR encapsulated in an intact outer RPE tissue emerged on D24, while our model underwent a delayed invagination process from D24 to D38. The expression of SCF in adjacent RPE suggested that RPE served as a supporting tissue for the CMZ by providing SCF(Fig.S2E), which indicated the prolonged invagination may result from the polarized distribution of RPE and NR of our retinal organoids. More interestingly, compared with the phosphorylation level of SCFR in the central NR, the activation of SCFR was always relatively limited in the CMZ even though the exogenous SCF was added(Fig. S2I,L). This is contradictory with the high expression of SCFR in the CMZ. We speculated that the activation of SCFR in the CMZ is more complex than that in the central NR. Co-activation with other receptors or cell-cell contact activation of SCFR in the CMZ may be considered in future investigation(Lennartsson and Ronnstrand, 2012;Mellough et al., 2015;Oakie et al., 2019).

From fish to mammals, the RGC has consistently been shown to be the earliest retinal cell type generated by RPCs occupying the inner neuroblast cell layer(Heavner and Pevny, 2012). In the CNS, Nestin[+] neural stem cells construct a scaffold-like structure, which provides a path for Tuj1^{+} neurons to climb from the apical side toward the basal side of the neural epithelium(Xu et al., 2013;Xu et al., 2015). Moreover, previous reports have shown that SCFR signaling can promote the migration and axonal extension of the CNS neurons (Guijarro et al., 2013;Sun et al., 2004). In current report, we identified a similar pro-migration effect of SCF/SCFR signaling on RGC generation in the central-most region of the NR, which might further develop into the fovea(Hoshino et al., 2017). In addition, we found that cellular apoptosis in the NR was dramatically repressed after activation of SCFR and this result could be antagonized by the inhibitor of SCFR. During development of the retina, far more neurons are generated than are ultimately needed, with almost one half of them undergoing programmed cell death shortly before establishing meaningful contacts within their targets(Vecino and Acera, 2015). This repression of apoptosis could further perturb the normal development of neural circuit formation and disturb cell death-related morphogenesis, resulting in congenital amblyopia, optic nerve hypoplasia or even retina degeneration (Teng and Toyama, 2011;Toyama et al., 2008). Considering the important function of migration, cell cycle length, and apoptosis in the genesis of neuro-retina, the SCF/SCFR signaling may exert multiple functions and mechanisms

in the neurogenesis and morphogenesis of the human embryonic eye by connecting multiple fundamental cell behaviors.

The application of SCFR in the translational medicine is also of great interest recent years. As a cell surface antigen, SCFR could act as a sorting strategy to enrich the qualified donor retinal progenitor cells for the retinitis pigmentosa (RP) disease. The SCFR^{+} donor cells survive up to 6 months in the subretinal space of host retina without generating teratoma. More importantly, in addition to robust material transfer and perfect cell replacement, these donor cells greatly inhibit the activation of microglia cells and improve the immune microenvironment of the RP disease(Chen et al., 2016;Zou et al., 2019). Our data well support the idea of SCFR[+] RPCs from a developmental view and partially explain for the advantages for transplantation such as retinal multipotency, limited proliferation, strong survive ability, and proper migration. In addition to the role in the light-sensing neuro-retina, we demonstrated that the SCF/SCFR signaling also participate in the development of ocular refractive system: regulate the growth of axial length by shaping the CMZ at embryonic stage, a similar story in the light-guided retina growth of chicken retina(Fischer et al., 2013).

As SCF/SCFR signaling broadly involved with the early development of embryonic eye, the downstream target of the SCF/SCFR signaling pathway should be investigated. For retinal neurogenesis, the mTOR pathway could be an intriguing target to take into consideration as it is proved robustly involving the neurogenesis in both the CMZ and the central NR(Choi et al., 2018;Love et al., 2014;Saxton and Sabatini, 2017;Zelinka et al., 2016). In the meantime, the PI3K-mTOR pathway has been proved a main downstream of the SCF/SCFR signaling and we also detected a considerate positive signal of active mTOR (data not shown). Moreover, the overactivation and inhibition of SCF/SCFR signaling led to a different extent between neurogenesis and gliogenesis in the central NR. This data clued that the SCF/SCFR signaling may be involved in modulation of intrinsic retinal developmental gene such as Lhx2(de Melo et al., 2018). Other classic pathways of neural development, such as Wnt, Notch, and Hedgehog signaling, may also crosstalk with SCF/SCFR signaling as reported in other organ development or disease pathophysiology(Ahmad et al., 2004). The regulation of SCFR itself is also an interesting topic. As the previous report said, AP2-α, the transcription factor that binds the promoter of the SCFR gene, plays a critical role in the development of the optic stalk and the lens and OC patterning in the developing retina (Bassett et al., 2010;West-Mays et al., 1999). The basic helix-loop-helix transcription factor microphthalmia associated transcription factor(MITF) ,which is the key marker of RPE development, is an important regulator of SCFR expression in mast cells and melanocytes(Opdecamp et al., 1997;Tsujimura et al., 1996). Interestingly, there is also an inverse regulation in that SCFR signaling regulates MITF expression through miRNAs miR-539 and miR-

381(Lee et al., 2011). Combined with the specific expression of SCFR in the MITF negative peripheral NR which tightly adjacent to the MITF positive RPE, we can predict an interesting relationship could exist between SCFR and MITF in this hinge-like region of optic cup.

To summarize, as an extrinsic environmental signal, SCF/SCFR signaling may serve as one of the mechanisms by which tissue-tissue interactions might be utilized in eye development (Fig. 7). However, lots of problems need to be explored in the field. Does the SCF/SCFR signaling involve with the epithelial flow into the OC (Heermann et al., 2015) during the eye morphogenesis? Does the expression of SCFR differ from the different ocular axis during the early development of eye? What is the regulatory molecular mechanism of SCFR expression dynamics in the developing retina? In the future, answering these questions is of great interest to better understand human eye development and promote clinical applications in treating human congenital eye disease.

Materials and Methods

Human embryonic stem cell culture

All experiments were performed in accordance with the guidelines of the Ethics Committee of Southwest Hospital, The Army Medical University. The hESC Line H1 (RRID:CVCL_9771) were used in this research. Briefly, hESCs were cultured under feeder-free condition using Essential 8^{TM} Medium (Gibco) and Vitronectin (Gibco). For routine culture, hESCs colonies were passaged every 4~5 days using Versene (Gibco) at 37℃ for 5 min. The detached hESC clumps were broken into small pieces by gentle pipetting. Morphologically identifiable differentiated cells were mechanically removed at each passage.

Retinal differentiation of hESCs and administration of SCF and isck03

The 3D human OC culture (SFEBq culture) was performed as previously described (Kuwahara et al., 2015). hESCs were dissociated into single cells in TrypLE Express (Gibco) and quickly reaggregated using low-cell adhesion 96-well plates with V-bottomed conical wells (Sumitomo Bakelite) in 3D OC differentiation medium (10,000 cells per well) supplemented with 20 mM Y-27632 (Sigma) under 5% CO_2 at 37℃. The differentiation medium contained 45% Iscove's modified Dulbecco's medium (IMDM, Gibco), 45% Hams F12 (F12, Gibco), Glutamax, 1% chemically defined lipid concentrate (Gibco), 10% Knockout Serum Replacement (KSR) (Gibco), monothioglycerol (450 μM, Sigma), 100 U ml^{-1} penicillin and 100 μg ml^{-1} streptomycin (Gibco). Recombinant human BMP4 (PeproTech) was added to the culture at a final concentration of 1.5 nM (55 ng/ml) on D6, and half of the medium was changed every 3rd day. The 3D retinal organoids were transferred to 9-cm

Petri dishes (ultra-low adhesion, Corning) at D18 for further culture in suspension with long-term culture medium containing DMEM/F12-Glutamax medium (Gibco), 1% N2 supplement (Gibco), 10% fetal bovine serum (FBS), 0.5 μM retinoic acid (Sigma), 0.1 mM taurine (Sigma), 0.25 μg ml^{-1} Fungizone (Gibco), 100 U ml^{-1} penicillin and 100 μg ml^{-1} streptomycin (Gibco). Standard 3D OCs with both the NR and the RPE at D24 were collected in the experimental groups. Recombinant human SCF (R & D) and isck03 (Abcam) was added to the 3D culture during D24~D30 at a final concentration of 20 ng/ml and 100 μM, respectively.

BrdU labeling assay

BrdU labeling was performed at different time courses, as indicated in the results. 3D OCs were cultured in long-term culture medium in the presence of BrdU (5 μg ml^{-1}, 16 μM; Sigma). Then, aggregates were washed with medium and cultured in the absence of BrdU for the BrdU dilution experiment or directly fixed for the BrdU incorporation experiment.

Immunofluorescence and confocal microscopy

Immunofluorescence was performed as previously described (Lakowski et al., 2018). Retinal organoids and human fetal retinae were fixed in 4% (wt/vol) phosphate-buffered formaldehyde solution at 4°C for 15–30 minutes, washed three times with PBS and equilibrated in 30% (wt/vol) sucrose solution at 4°C overnight. Specimens were then transferred into an optimal cutting temperature (OCT)- compound (Biosharp) and frozen in a -80°C refrigerator. A Leica CM1900UV cryostat was used to produce 10 μm thick sections. For immunofluorescence analysis, optimal cutting temperature (OCT) compound was removed by a 15-minute incubation at 37°C with PBS, and cryosections were blocked with 10% (vol/vol) FBS and 1% (wt/vol) bovine serum albumin (BSA) in PBS containing 0.1% (vol/vol) Triton X-100 for one hour at room temperature. The following primary antibodies were used in the same blocking solution for 1 hour at room temperature and 4°C overnight. Rax (1:500; Abcam), MITF (1:400; Abcam), Pax6 (1:500; Abcam), Chx10 (1:500; Abcam), Sox2 (1:500; Abcam), SSEA4 (1:500; Abcam), Ki67 (1:500; Cell Signaling Technology), Nestin (1:200; Sigma-Aldrich), p27Kip1 (1:500; Abcam), SSEA1 (1:400; Cell Signaling Technology), AQP1 (1:500; Novus), SCFR (1:400; Cell Signaling Technology), Anti-BrdU (1:100; Sigma-Aldrich), pMLC (1:200; Abcam), ZO-1(1:400; Cell Signaling Technology), Phalloidin (1:500; Sigma-Aldrich), Brn3b (1:200; Abcam), Tuj1 (1:200 Cell; Signaling Technology), cleaved-caspase3 (1:500; Cell Signaling Technology), Islet1(1:500; Abcam), Anti-

SCF(1:400; Abcam), anti-p-SCFR(1:300; Abcam), Vsx2(1:1000; Sigma-Aldrich), Calretinin(1:1000; Millipore), CRALBP(1:400; Abcam). The primary antibody was omitted for negative controls. Primary antibody staining was followed by three washes with 1x PBS. Subsequently, cryosections were incubated for 1 hour at room temperature with the appropriate secondary antibody (goat anti-rabbit Alexa Fluor 488, Invitrogen; goat anti-rabbit Alexa Fluor 594, Invitrogen; goat anti-mouse Alexa Fluor 488, Invitrogen; goat anti-mouse Alexa Fluor 594, Invitrogen;all 1:1000) diluted in blocking solution. DAPI (1:10, Beyotime) was applied for 10 minutes at room temperature to counterstain nuclei, followed by three washes with PBS prior to cover-slipping with the antifade mounting medium (Beyotime).

Microscopy, image acquisition, and processing

A Zeiss LSM880 was used for the acquisition of confocal images. Images were processed in Zen2.3 (blue edition, Zeiss), FIJI, Photoshop CC 2017 (Adobe), and Illustrator CC 2017 (Adobe).

Quantification of the RPE-NR angle, the axial length, and the CMZ length

A Leica DMI3000 was used for the acquisition of bright field images of 3D retinal organoids. The NR-RPE angle, the axial length, and the CMZ length were measured by ImageJ as indicated in Figure3a,d. Note that region of the CMZ was identified by the RPE-NR boundary and the position where the inner cell layer emerges in the bright field.

Real-time polymerase chain reaction (RT-PCR)

Three independent *in vitro* experiments were performed. Briefly, total RNA was extracted from 3D human OCs with TRIzol reagent (Gibco), and RNA was reverse-transcribed using the PrimeScript® RT Reagent Kit (Takara). The cDNA was amplified with specific gene primers. Quantitative RT-PCR was conducted using the CFX96 Real-Time PCR System (Bio-Rad) with at least three separate RNA samples. Rax, For AACCGCACGACTTTCACCAC, Rev TGCAGCTTCATGGAGGACAC; LHX2, For GCGATGCTGTTCCACAGTCT, Rev TAGCGGTCCGAGATCTTGCC; Pax6, For CCAGGGCAATCGGTGGTAGT, Rev GCTAGCCAGGTTGCGAAGAA; OCT4, For GACAGGGGGAGGGGAGGAGCTAGG, Rev CTTCCCTCCAACCAGTTGCCCCAAAC; SOX2, For TTACGCGCACATGAACGGCT, Rev TGCGAGTAGGACATGCTGTA; SCFR, For TCCCAGAGCCCACAATAG, Rev GAAGTCTTGCCCACATCG; GAPDH, For

CCATGTTCGTCATGGGTGTGA, Rev CATGAGTCCTTCCACGATACCA.

Statistical analysis

Data were presented as means ± s.e.m. Statistical tests were performed with the PRISM software (GraphPad, version 6.01). Statistical significance was tested with Student's t-test (parametric) and ANOVA with Tukey's or Dunnett's correction was used for multiple comparisons. A P-value <0.05 was considered significant.

Competing Interests:

All authors declare no competing or financial interests.

Author Contributions:

Conceptualization: Y.G., X.H.; Methodology: Q.L.,Y.L.,L.G.,Y.Z.; Validation: H.X.,J.H.,B.B.; Formal analysis: Y.G., X.H.; Investigation: Y.G.,H.X.; Resources: Q.L., Y.Z.; Data curation: Y.G., H.H.; Writing-original draft:Y.G.; Writing-review & editing: H.X.,Z.Q.Y.; Supervision: H.X.,Z.Q.Y.; Project administration: H.X.,Z.Q.Y.; Funding acquisition: H.X.,Z.Q.Y.

References:

Agathocleous, M. and Harris, W. A. (2009). From progenitors to differentiated cells in the vertebrate retina. *Annu Rev Cell Dev Biol*. **25**, 45-69.

Ahmad, I., Das, A. V., James, J., Bhattacharya, S. and Zhao, X. (2004). Neural stem cells in the mammalian eye: types and regulation. *Semin Cell Dev Biol*. **15(1)**, 53-62.

Bassett, E. A. and Wallace, V. A. (2012). Cell fate determination in the vertebrate retina. *Trends Neurosci*. **35(9)**, 565-573.

Bassett, E. A., Williams, T., Zacharias, A. L., Gage, P. J., Fuhrmann, S. and West-Mays, J. A. (2010). AP-2alpha knockout mice exhibit optic cup patterning defects and failure of optic stalk morphogenesis. *Hum Mol Genet*. **19(9)**, 1791-1804.

Belanger, M. C., Robert, B. and Cayouette, M. (2017). Msx1-Positive Progenitors in the Retinal Ciliary Margin Give Rise to Both Neural and Non-neural Progenies in Mammals. *Dev Cell*. **40(2)**, 137-150.

Cayouette, M., Poggi, L. and Harris, W. A. (2006). Lineage in the vertebrate retina. *Trends Neurosci*. **29(10)**, 563-570.

Cayouette, M. and Raff, M. (2003). The orientation of cell division influences cell-fate choice in the developing mammalian retina. *Development*. **130(11)**, 2329-2339.

Chen, S., Li, H., Gaudenz, K., Paulson, A., Guo, F., Trimble, R., Peak, A., Seidel, C., Deng, C., Furuta, Y., et al. (2013). Defective FGF signaling causes coloboma formation and disrupts retinal neurogenesis. *Cell Res*. **23(2)**, 254-273.

Chen, X., Chen, Z., Li, Z., Zhao, C., Zeng, Y., Zou, T., Fu, C., Liu, X., Xu, H. and Yin, Z. Q. (2016). Grafted c-kit+/SSEA1- eye-wall progenitor cells delay retinal degeneration in mice by regulating neural plasticity and forming new graft-to-host synapses. *Stem Cell Res Ther*. **7(1)**, 191.

Choi, J.-H., Jo, H. S., Lim, S., Kim, H.-T., Lee, K. W., Moon, K. H., Ha, T., Kwak, S. S., Kim, Y., Lee, E. J., et al. (2018). mTORC1 accelerates retinal development via the immunoproteasome. *Nat Commun*. **9(1)**, 2502.

Das, A. V., Edakkot, S., Thoreson, W. B., James, J., Bhattacharya, S. and Ahmad, I. (2005a). Membrane properties of retinal stem cells/progenitors. *Prog Retin Eye Res*. **24(6)**, 663-681.

Das, A. V., James, J., Rahnenfuhrer, J., Thoreson, W. B., Bhattacharya, S., Zhao, X. and Ahmad, I. (2005b). Retinal properties and potential of the adult mammalian ciliary epithelium stem cells. *Vision Res*. **45(13)**, 1653-1666.

Das, T., Payer, B., Cayouette, M. and Harris, W. A. (2003). In vivo time-lapse imaging of cell divisions during neurogenesis in the developing zebrafish retina. *Neuron*. **37(4)**, 597-609.

de Melo, J., Clark, B. S. and Venkataraman, A. (2018). Ldb1- and Rnf12-dependent regulation of Lhx2 controls the relative balance between neurogenesis and gliogenesis in the retina. *Development*. **145(9)**, dev159970.

Dyer, M. A. and Cepko, C. L. (2001). p27Kip1 and p57Kip2 regulate proliferation in distinct retinal progenitor cell populations. *J Neurosci*. **21(12)**, 4259-4271.

Eiraku, M., Adachi, T. and Sasai, Y. (2012). Relaxation-expansion model for self-driven retinal morphogenesis: a hypothesis from the perspective of biosystems dynamics at the multi-cellular level. *Bioessays*. **34(1)**, 17-25.

Eiraku, M., Takata, N., Ishibashi, H., Kawada, M., Sakakura, E., Okuda, S., Sekiguchi, K., Adachi, T. and Sasai, Y. (2011). Self-organizing optic-cup morphogenesis in three-dimensional culture. *Nature*. **472(7341)**, 51-56.

Fischer, A. J., Bosse, J. L. and El-Hodiri, H. M. (2013). The ciliary marginal zone (CMZ) in development and regeneration of the vertebrate eye. *Exp Eye Res*. **116**, 199-204.

Fuhrmann, S. (2010). Eye morphogenesis and patterning of the optic vesicle. *Curr Top Dev Biol*. **93**, 61-84.

Guijarro, P., Wang, Y., Ying, Y., Yao, Y., Jieyi, X. and Yuan, X. (2013). In vivo knockdown of cKit impairs neuronal migration and axonal extension in the cerebral cortex. *Dev Neurobiol*. **73(12)**, 871-887.

Harris, W. A. and Perron, M. (1998). Molecular recapitulation: the growth of the vertebrate retina. *Int J Dev Biol*. **42(3)**, 299-304.

Hasegawa, T., McLeod, D. S., Prow, T., Merges, C., Grebe, R. and Lutty, G. A. (2008). Vascular precursors in developing human retina. *Invest Ophthalmol Vis Sci*. **49(5)**, 2178-2192.

Heavner, W. and Pevny, L. (2012). Eye development and retinogenesis. *Cold Spring Harb Perspect Biol*. **4(12)**, a008391.

Heermann, S., Schutz, L., Lemke, S., Krieglstein, K. and Wittbrodt, J. (2015). Eye morphogenesis driven by epithelial flow into the optic cup facilitated by modulation of bone morphogenetic protein. *Elife*. **4**.

Heinrich, M. C., Blanke, C. D., Druker, B. J. and Corless, C. L. (2002). Inhibition of KIT tyrosine kinase activity: a novel molecular approach to the treatment of KIT-positive malignancies. *J Clin Oncol*. **20(6)**, 1692-1703.

Hirota, S., Isozaki, K., Moriyama, Y., Hashimoto, K., Nishida, T., Ishiguro, S., Kawano, K., Hanada, M., Kurata, A., Takeda, M., et al. (1998). Gain-of-function mutations of c-kit in human gastrointestinal stromal tumors. *Science*. **279(5350)**, 577-580.

Hoshino, A., Ratnapriya, R., Brooks, M. J., Chaitankar, V., Wilken, M. S., Zhang, C., Starostik, M. R., Gieser, L., La Torre, A., Nishio, M., et al. (2017). Molecular Anatomy of the Developing Human Retina. *Dev Cell*. **43(6)**, 763-779.e764.

Keshet, E., Lyman, S. D., Williams, D. E., Anderson, D. M., Jenkins, N. A., Copeland, N. G. and Parada, L. F. (1991). Embryonic RNA expression patterns of the c-kit receptor and its cognate ligand suggest multiple functional roles in mouse development. *EMBO J*. **10(9)**, 2425-2435.

Koso, H., Iida, A., Tabata, Y., Baba, Y., Satoh, S., Taketo, M. M. and Watanabe, S. (2008). CD138/syndecan-1 and SSEA-1 mark distinct populations of developing ciliary epithelium that are regulated differentially by Wnt signal. *Stem Cells*. **26(12)**, 3162-3171.

Koso, H., Satoh, S. and Watanabe, S. (2007). c-kit marks late retinal progenitor cells and regulates their differentiation in developing mouse retina. *Dev Biol*. **301(1)**, 141-154.

Kuwahara, A., Ozone, C., Nakano, T., Saito, K., Eiraku, M. and Sasai, Y. (2015). Generation of a ciliary margin-like stem cell niche from self-organizing human retinal tissue. *Nat Commun*. **6**, 6286.

Lakowski, J., Welby, E., Budinger, D., Di Marco, F., Di Foggia, V., Bainbridge, J. W. B., Wallace, K. and Gamm, D. M. (2018). Isolation of Human Photoreceptor Precursors via a Cell Surface Marker Panel from Stem Cell-Derived Retinal Organoids and Fetal Retinae. *Stem Cells*. **36(5)**, 709-722.

Larsen, K. B., Lutterodt, M., Rath, M. F. and Moller, M. (2009). Expression of the homeobox genes PAX6, OTX2, and OTX1 in the early human fetal retina. *Int J Dev Neurosci*. **27(5)**, 485-492.

Lee, Y. N., Brandal, S., Noel, P., Wentzel, E., Mendell, J. T., McDevitt, M. A., Kapur, R., Carter, M., Metcalfe, D. D. and Takemoto, C. M. (2011). KIT signaling regulates MITF expression through miRNAs in normal and malignant mast cell proliferation. *Blood*. **117(13)**, 3629-3640.

Lennartsson, J. and Ronnstrand, L. (2012). Stem cell factor receptor/c-Kit: from basic science to clinical implications. *Physiol Rev.* **92(4)**, 1619-1649.

Livesey, F. J. and Cepko, C. L. (2001). Vertebrate neural cell-fate determination: lessons from the retina. *Nat Rev Neurosci.* **2(2)**, 109-118.

Love, N. K., Keshavan, N., Lewis, R., Harris, W. A. and Agathocleous, M. (2014). A nutrient-sensitive restriction point is active during retinal progenitor cell differentiation. *Development.* **141(3)**, 697-706.

Lowe, A., Harris, R., Bhansali, P., Cvekl, A. and Liu, W. (2016). Intercellular Adhesion-Dependent Cell Survival and ROCK-Regulated Actomyosin-Driven Forces Mediate Self-Formation of a Retinal Organoid. *Stem Cell Reports.* **6(5)**, 743-756.

Matsui, Y., Zsebo, K. M. and Hogan, B. L. (1990). Embryonic expression of a haematopoietic growth factor encoded by the SI locus and the ligand for c-kit. *Nature.* **347(6294)**, 667-669.

Mellough, C. B. and Bauer, R. (2019). An integrated transcriptional analysis of the developing human retina. *Development.* **146(2)**, dev169474.

Mellough, C. B., Collin, J., Khazim, M., White, K., Sernagor, E., Steel, D. H. and Lako, M. (2015). IGF-1 Signaling Plays an Important Role in the Formation of Three-Dimensional Laminated Neural Retina and Other Ocular Structures From Human Embryonic Stem Cells. *Stem Cells.* **33(8)**, 2416-2430.

Nakano, T., Ando, S., Takata, N., Kawada, M., Muguruma, K., Sekiguchi, K., Saito, K., Yonemura, S., Eiraku, M. and Sasai, Y. (2012). Self-formation of optic cups and storable stratified neural retina from human ESCs. *Cell Stem Cell.* **10(6)**, 771-785.

O'Brien, K. M., Schulte, D. and Hendrickson, A. E. (2003). Expression of photoreceptor-associated molecules during human fetal eye development. *Mol Vis*. **9**, 401-409.

Oakie, A., Feng, Z. C., Li, J., Silverstein, J., Yee, S. P. and Wang, R. (2019). Long-term c-Kit overexpression in beta cells compromises their function in ageing mice. *Diabetologia*. **62(8)**, 1430-1444.

Opdecamp, K., Nakayama, A., Nguyen, M. T., Hodgkinson, C. A., Pavan, W. J. and Arnheiter, H. (1997). Melanocyte development in vivo and in neural crest cell cultures: crucial dependence on the Mitf basic-helix-loop-helix-zipper transcription factor. *Development*. 124(12), 2377-2386.

Pasca, S. P. (2018). The rise of three-dimensional human brain cultures. *Nature*. **553(7689)**, 437-445.

Picker, A. and Brand, M. (2005). Fgf signals from a novel signaling center determine axial patterning of the prospective neural retina. *Development*. **132(22)**, 4951-4962.

Pilaz, L. J., McMahon, J. J., Miller, E. E., Lennox, A. L., Suzuki, A., Salmon, E. and Silver, D. L. (2016). Prolonged Mitosis of Neural Progenitors Alters Cell Fate in the Developing Brain. *Neuron*. **89(1)**, 83-99.

Rossi, G., Manfrin, A. and Lutolf, M. P. (2018). Progress and potential in organoid research. *Nat Rev Genet*. **19(11)**, 671-687.

Sasai, Y. (2013). Cytosystems dynamics in self-organization of tissue architecture. *Nature*. **493(7432)**, 318-326.

Saxton, R. A. and Sabatini, D. M. (2017). mTOR Signaling in Growth, Metabolism, and Disease. *Cell*. **168(6),** 960-976.

Sun, L., Lee, J. and Fine, H. A. (2004). Neuronally expressed stem cell factor induces neural stem cell migration to areas of brain injury. *J Clin Invest*. **113(9)**, 1364-1374.

Teng, X. and Toyama, Y. (2011). Apoptotic force: active mechanical function of cell death during morphogenesis. *Dev Growth Differ.* **53(2)**, 269-276.

Toyama, Y., Peralta, X. G., Wells, A. R., Kiehart, D. P. and Edwards, G. S. (2008). Apoptotic force and tissue dynamics during Drosophila embryogenesis. *Science.* **321(5896)**, 1683-1686.

Tsujimura, T., Morii, E., Nozaki, M., Hashimoto, K., Moriyama, Y., Takebayashi, K., Kondo, T., Kanakura, Y. and Kitamura, Y. (1996). Involvement of transcription factor encoded by the mi locus in the expression of c-kit receptor tyrosine kinase in cultured mast cells of mice. *Blood.* **88(4)**, 1225-1233.

Valdivia, L. E., Lamb, D. B., Horner, W., Wierzbicki, C., Tafessu, A., Williams, A. M., Gestri, G., Krasnow, A. M., Vleeshouwer-Neumann, T. S., Givens, M., et al. (2016). Antagonism between Gdf6a and retinoic acid pathways controls timing of retinal neurogenesis and growth of the eye in zebrafish. *Development.* **143(7)**, 1087-1098.

Vecino, E. and Acera, A. (2015). Development and programed cell death in the mammalian eye. *Int J Dev Biol.* **59(1-3)**, 63-71.

Wang, H., Zhuang, X., Cai, Y., Cheung, A. Y. and Jiang, L. (2013). Apical F-actin-regulated exocytic targeting of NtPPME1 is essential for construction and rigidity of the pollen tube cell wall. *Plant J.* **76(3)**, 367-379.

West-Mays, J. A., Zhang, J., Nottoli, T., Hagopian-Donaldson, S., Libby, D., Strissel, K. J. and Williams, T. (1999). AP-2alpha transcription factor is required for early morphogenesis of the lens vesicle. *Dev Biol.* **206(1)**, 46-62.

Woodman, S. E. and Davies, M. A. (2010). Targeting KIT in melanoma: a paradigm of molecular medicine and targeted therapeutics. *Biochem Pharmacol.* **80(5)**, 568-574.

Xu, H., Yang, Y., Tang, X., Zhao, M., Liang, F., Xu, P., Hou, B., Xing, Y., Bao, X. and Fan, X. (2013). Bergmann glia function in granule cell migration during cerebellum development. *Mol Neurobiol.* **47(2)**, 833-844.

Xu, L., Tang, X., Wang, Y., Xu, H. and Fan, X. (2015). Radial glia, the keystone of the development of the hippocampal dentate gyrus. *Mol Neurobiol.* **51(1)**, 131-141.

Xue, X. Y. and Harris, W. A. (2012). Using myc genes to search for stem cells in the ciliary margin of the Xenopus retina. *Dev Neurobiol.* **72(4)**, 475-490.

Yamaguchi, Y., Watanabe, T., Hirakata, A. and Hida, T. (2006). Localization and ontogeny of aquaporin-1 and -4 expression in iris and ciliary epithelial cells in rats. *Cell Tissue Res.* **325(1)**, 101-109.

Zelinka, C. P., Volkov, L., Goodman, Z. A., Todd, L., Palazzo, I., Bishop, W. A. and Fischer, A. J. (2016). mTor signaling is required for the formation of proliferating Müller glia-derived progenitor cells in the chick retina. *Development.* **143(11)**, 1859-1873.

Zhong, W. and Chia, W. (2008). Neurogenesis and asymmetric cell division. *Curr Opin Neurobiol.* **18(1)**, 4-11.

Zhong, X., Gutierrez, C., Xue, T., Hampton, C., Vergara, M. N., Cao, L. H., Peters, A., Park, T. S., Zambidis, E. T., Meyer, J. S., et al. (2014). Generation of three-dimensional retinal tissue with functional photoreceptors from human iPSCs. *Nat Commun.* **5**, 4047.

Zhou, P. Y., Peng, G. H., Xu, H. and Yin, Z. Q. (2015). c-Kit(+) cells isolated from human fetal retinas represent a new population of retinal progenitor cells. *J Cell Sci*. **128(11)**, 2169-2178.

Zigman, M., Cayouette, M., Charalambous, C., Schleiffer, A., Hoeller, O., Dunican, D., McCudden, C. R., Firnberg, N., Barres, B. A., Siderovski, D. P., et al. (2005). Mammalian inscuteable regulates spindle orientation and cell fate in the developing retina. *Neuron*. **48(4)**, 539-545.

Zou, T., Gao, L., Zeng, Y., Li, Q., Li, Y., Chen, S., Hu, X., Chen, X., Fu, C. and Xu, H. (2019). Organoid-derived C-Kit(+)/SSEA4(-) human retinal progenitor cells promote a protective retinal microenvironment during transplantation in rodents. *Nat Commun*. **10(1)**, 1205.

Figures
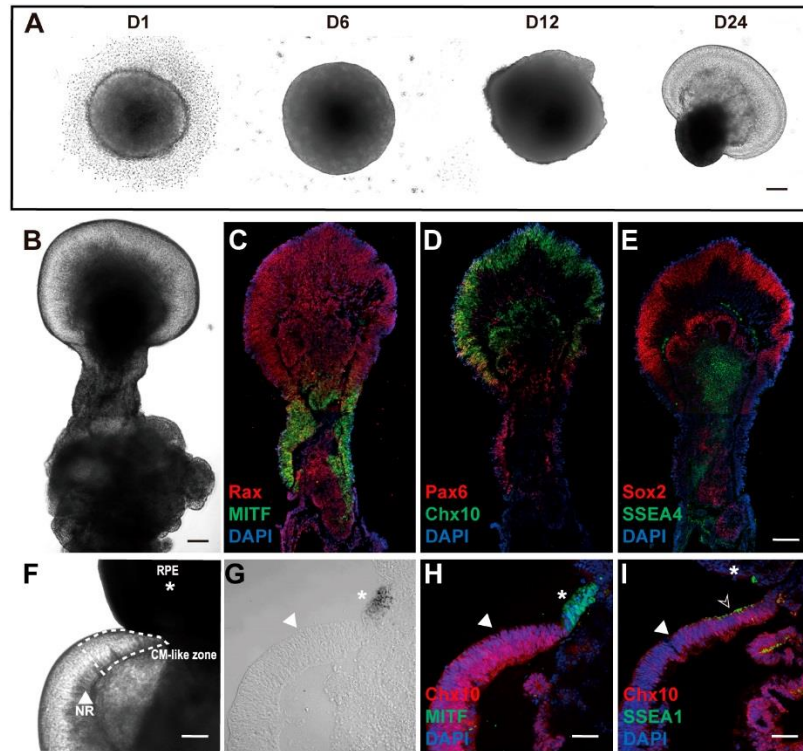
Figure 1. Generation of hESC-derived OCs with the CMZ

(A) Phase-contrast microscopy images of the 3D human OC at different developmental time points(D1,D6,D12,D24), showing the sequential morphological changes from embryonic body (D1) to OC (D24).

(B-E) Bright field view(B) and immunostaining of 3D human OCs at D24 for Rax, MITF (C); Pax6, Chx10 (D); Sox2, SSEA4 (E) indicating the successful differentiation of 3D OC with both the NR (Rax, Pax6, Chx10, Sox2, SSEA4) and the RPE (MITF).

(F,G) Phase-contrast microscopy images of OCs at D30 show the typical morphology of the wedge-like CMZ and its unique location between the NR (white triangle) and RPE (asterisk).

(H) NR and RPE could be specifically stained with Chx10 (NR marker, red) and MITF (RPE marker, Green) with significant border.

(I) The limit of CMZ and NR is well dipicted by the double staining of SSEA1 and Chx10.

White triangle: NR; Asterisk: RPE; Blank arrowhead: CMZ; scale bars: 50 μm (F~I), 100 μm (A~E).
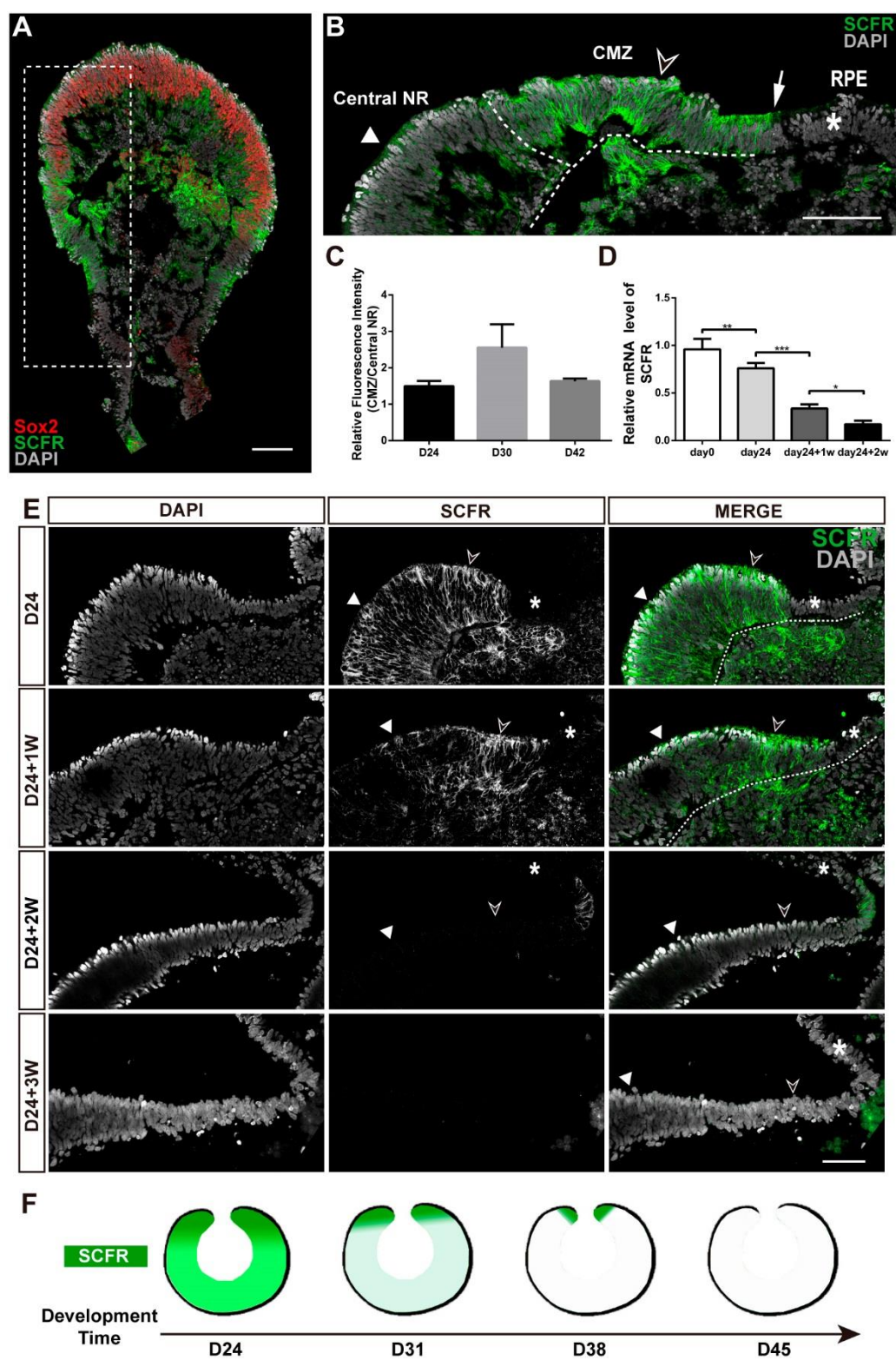
Figure 2. SCFR is strongly expressed and spatiotemporally confined in the CMZ of the human OC

(A,B) Immunostaining of the 3D human OC at D24 for SCFR and Sox2. B is a magnification of the region enclosed by the dashed box in A. Sox2 mainly distributed in the nonmarginal NR, while SCFR was expressed in the whole NR (white triangle) and CMZ (blank arrowhead) but not in the RPE (asterisk).

(C) Relative fluorescence intensity of SCFR of the CMZ versus central NR, showing an approximately 1.5~2.5 times fluorescence intensity in the CMZ than the central NR. (Mean±s.d.; n=9 for each time point, 3 independent experiments)

(D) RT-PCR analysis of the 3D humanOC from D0 to D38, showing the timely downregulation of SCFR expression in the 3D OC. (Mean±s.d.; n=9 for each time point, 3 independent experiments)

(E) Immunostaining of SCFR in the 3D human OC at D24, D31, D38, and D45. The expression of SCFR in the NR was confined to the CMZ in a temporal-spatial manner and diminished at D45.   White triangle: NR; Asterisk: RPE; Blank arrowhead: CMZ.

(F)Schematic of SCFR expression pattern of 3D human OC described in D.

*p < 0.05, **p < 0.01; ***p < 0.005. scale bars: 100 μm (A, B, E).
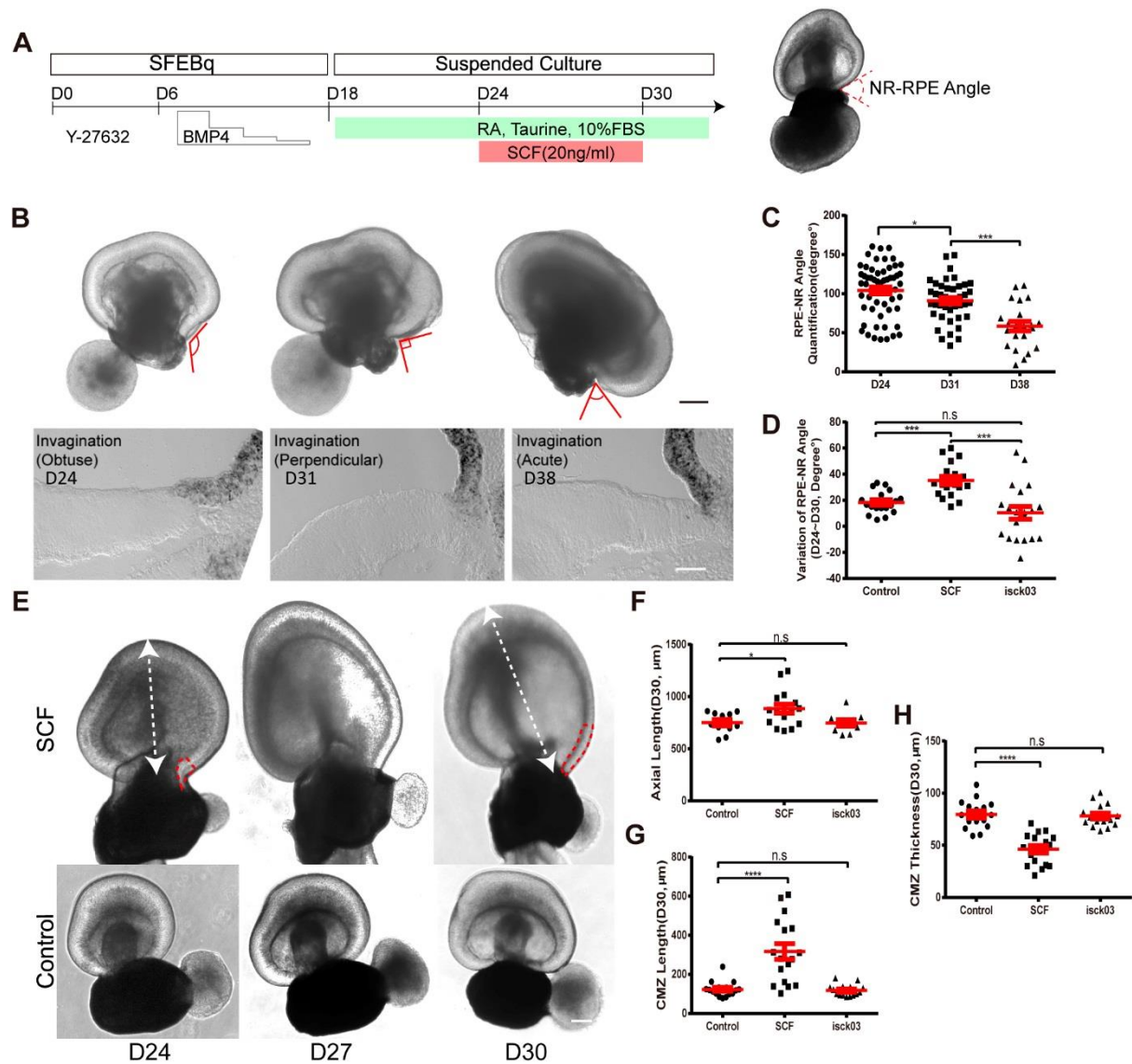
Figure 3. Activation of SCF/SCFR signaling facilitates NR invagination and increases the axial length

(A) Schematic of the experiment protocol of SCF treatment of the 3D human retinal organoid culture.

(B) Representative phase-contrast image of the 3D human optic with obtuse, perpendicular, and acute NR-RPE angles, showing invagination of the NR during OC morphogenesis.

(C) The quantification of the NR-RPE angle for each analyzed stage independently(n=59, 42, and 22 at each time point in 3 independent experiments).

(D) The variability of NR-RPE angle of control, SCF, and isck03 group between D24 and D30 (n=18, 18, and 20 for each group obtaining from 4 independent experiments).

(E) Phase-contrast images of the 3D human OC with and without SCF treatment at D24, D27, and D30. The white

dash line indicates the axial length. The red line bracket and the arrow indicate the CMZ.

(F-H) Quantification analysis of the axial length(n=11, 16, and 9), CMZ length(n=16, 17, and 15), and CMZ thickness(n=16, 15, and 15) of OCs, showing that SCF treatment significantly increased the axial length and the CMZ length. Data are shown as mean±S.E.M and collected from 3 independent experiments. Independent sample t test.*p < 0.05, **p < 0.01, ***p < 0.005, ****p < 0.001. Scale bars: 50 μm (B); 100 μm (E).
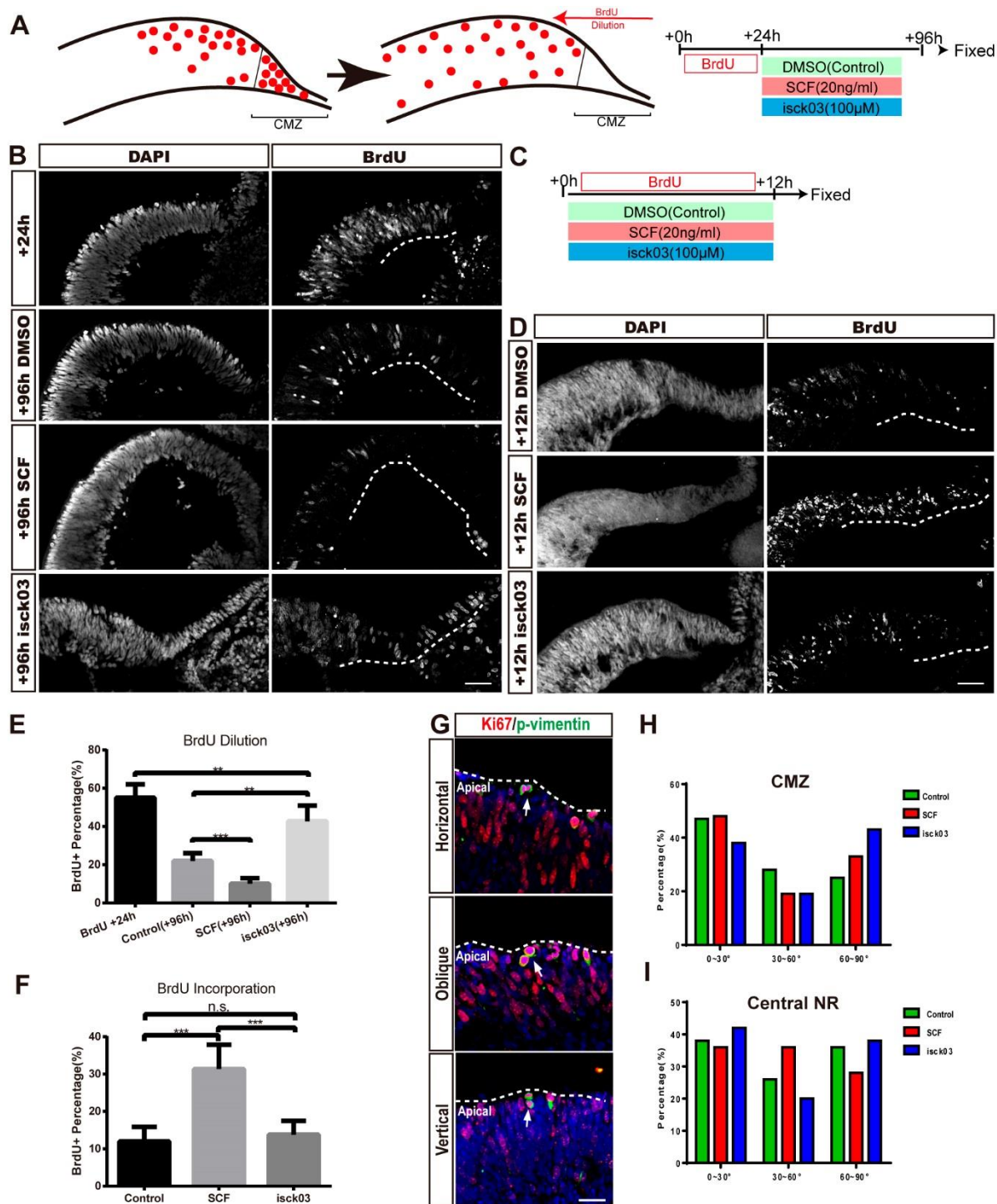
Figure 4. SCF/SCFR signaling orchestrates the cell cycle progression in the CMZ

(A) Schematic of BrdU dilution experiment of 3D human retinal oganoid. SCF, the SCFR ligand, and isck03, the

SCFR inhibitor were administrated for 72 hours after BrdU withdrawl.

(B) Immunostaining of the 3D OC for BrdU showing BrdU were abundant after incubation for 24 hours and more

rapidly diluted by SCF treatment in subsequent 72 hours. Dashed line indicates the CMZ. Scale bars, 50 µm.

(C) Schematic of BrdU incorporation experiment of 3D human OC.

(D) Immunostaining of the 3D OCs for BrdU after incubation for 12 hours with SCF or isck03 treatment. SCF treatment robustly increased BrdU incorporation in the CMZ and isck03 treatment gave reversed result. Scale bars, 50 µm.

(E) Quantification of BrdU$^+$ cells showing the BrdU dilution in the control and SCF treatment groups. (Mean±s.e.m; n=6 BrdU 24 h, n=12 controls, n=25 SCF, n=12 isck03, 3 independent experiments)

(F) Quantification of BrdU+ cells for BrdU incorporation in the control and SCF treatment group. (Mean±s.e.m; n=18 controls, n=12 SCF, n= 12 isck03, 3 independent experiments). Data are shown as mean±s.e.m. Independent sample t test. *p < 0.05, **p < 0.01; ***p < 0.005, ****p < 0.0001.

(G) Double staining of Ki67 and p-vimentin shows the typical spindle orientation of RPC mitotic divisions in the NR at D30. Scale bars: 20 µm.

(H,I) The statistics of each spindle orientation in the CMZ and NR shows that both the CMZ and central NR is mixed with three types of mitotic division and it is not altered by the administration of SCF and isck03. (P>0.05, 2x3 fisher exact test, n=81 for control, n=71 for SCF, n=106 for isck03, 3 independent experiments).
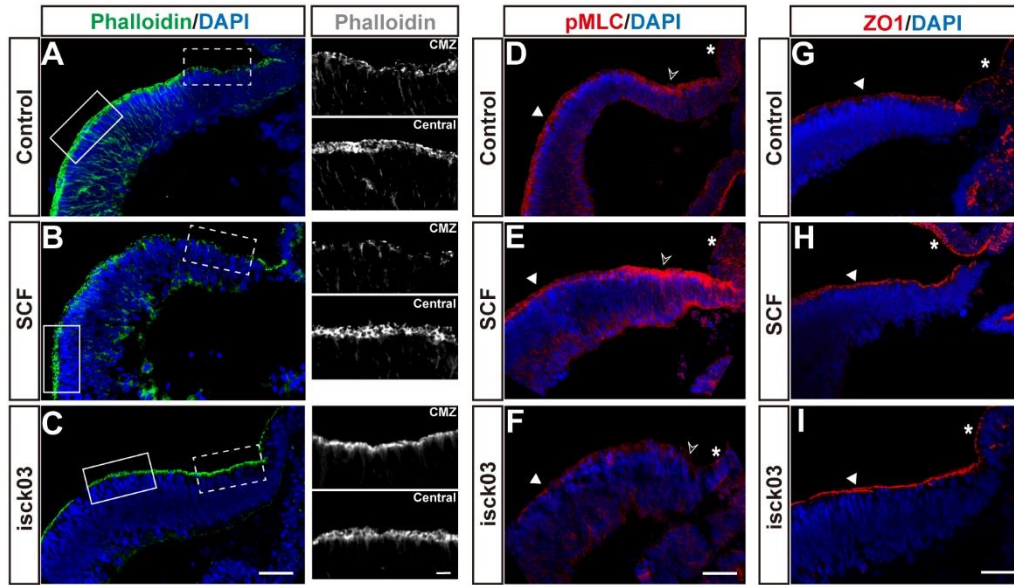
Figure 5. **SCF/SCFR signaling regulates cytoskeleton dynamics and apical constriction of the CMZ**

(A-C'') Immunostaining of the 3DOC of the control, SCF, and isck03 group at D30 for F-actin by phalloidin. Magnifications of the CMZ(top) were corresponded to the region of white dashed bracket and the central NR region(bottom) were corresponded to the region of white solid bracket. F-actin in the control and isck03 group was kept in a continuous manner both in the CMZ and the central NR while the SCF group was distributed in a noncontinuous manner in the CMZ and in a continuous but loose manner in the central NR. a-c, scale bars, 50 μm; magnifications, scale bars, 10 μm.

(D~F) Immunostaining of the 3D OCs at D30 for pMLC, showing that SCF treatment enhanced the activity of pMLC in the CMZ during invagination of the NR and isck03 decreased the activity of pMLC. The white triangle indicates the apical activity of pMLC in the CMZ. Scale bars, 50 μm.

(G~I) Immunostaining of the 3D OCs at D30 for ZO-1, showing that SCF and isck03 administration did not change the polarity of the NR. White triangle: NR; Asterisk: RPE; Blank arrowhead: CMZ. Scale bars, 50 μm.
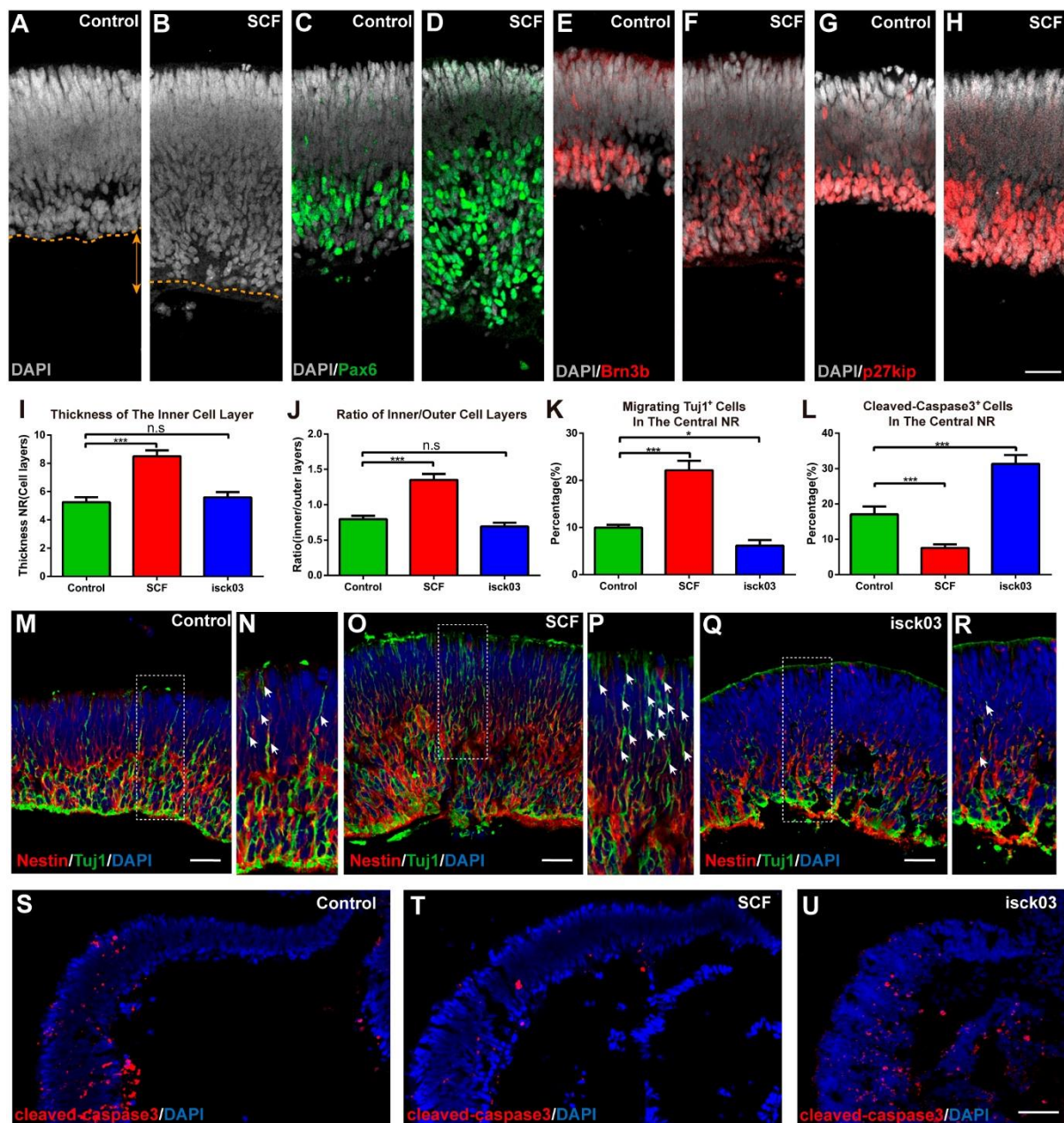
Figure 6. SCF/SCFR signaling accelerates the migration of immature ganglion cells and represses cellular apoptosis in the nonmarginal NR

(A and B) DAPI staining of the central-most NR at D30 showing thickening of the inner cell layer after SCF treatment. Brown dash line and the arrow indicate the difference of the inner cell layer thickness.

(C~H) Immunostaining of the central-most NR at D30 for Pax6 (C, D), Brn3b (E, F), and P27kip1 (G, H), showing robust accumulation of postmitotic ganglion cells in the inner cell layer. Scale bars, 25 μm.

(I and J) Quantification of the cell layers of the nonmarginal NR at D30 showing that SCF administration promoted the accumulation of cells in the inner cell layer (Mean±s.e.m; n=9 controls, n=9 SCF for each group, 3 independent experiments).

(K) Quantification of the migrating Tuj1+ ganglion cells at D30 in the central NR showing that SCF administration robustly promoted the accumulation of cells in the inner cell layer while isck03 block the migration.(Mean±s.e.m; n=9 controls, n=9 SCF for each group, 3 independent experiments).

(L) Quantification of cleaved-caspase3+ apoptotic cells in the NR in control, SCF-treated, and isck03-treated NR (Mean±s.e.m; n=9 controls, n= 9 SCF, n=9 isck03, 3 independent experiments).

(M~R) Immunostaining of the central-most NR for Nestin and Tuj1 at D30. N, P, and R are magnifications of the regions enclosed by the dashed boxes in M, O and Q, respectively. Significantly more Tuj1+ ganglion cells migrated in the NR in the SCF treated group than in the control group. Fewer Tuj1+ ganglion cells were observed in the isck03-treated NR. Scale bars, 50 μm.

(S~U) Immunostaining of the NR for cleaved-caspase3 showing that cell apoptosis in the NR was dramatically repressed by SCF inducement(T) and deteriorated by isck03 administration(U). Data are shown as mean±s.e.m. Independent sample t test. *p < 0.05, **p < 0.01; ***p < 0.005, ****p < 0.0001.Scale bars, 50 μm.
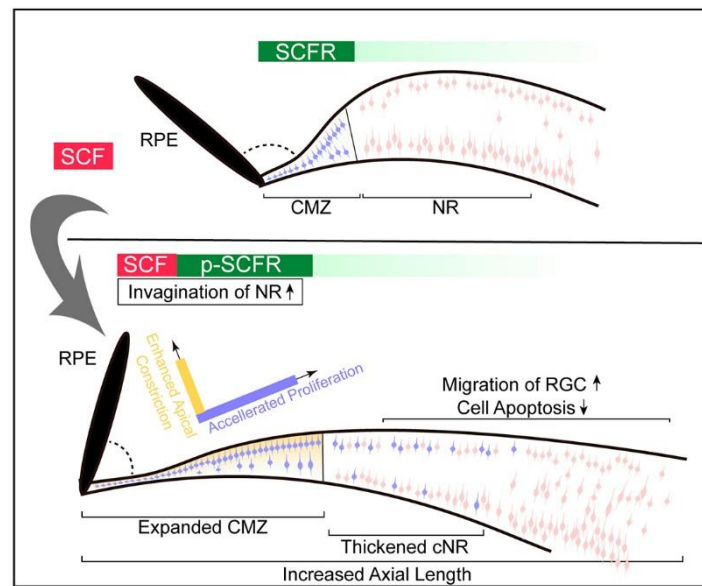
Figure 7. Schematic of the developmental role of SCF/SCFR signaling in the human embryonic neural retina

Activation of SCF/SCFR signaling provided a tangential power, which derived from the rapid proliferation of RSC/RPCs in the CMZ, and a vertical (centrifugal) power generated by the enhanced apical constriction. These powers pull the NR toward the rigid RPE and facilitated the invagination of NR. At the nonmarginal NR region, SCF promoted the migration of immature ganglion cells toward the basal side of the NR and repressed cell apoptosis in NR, thus produced a pro-neurogenesis effect during the early development of human embryonic neural retina.
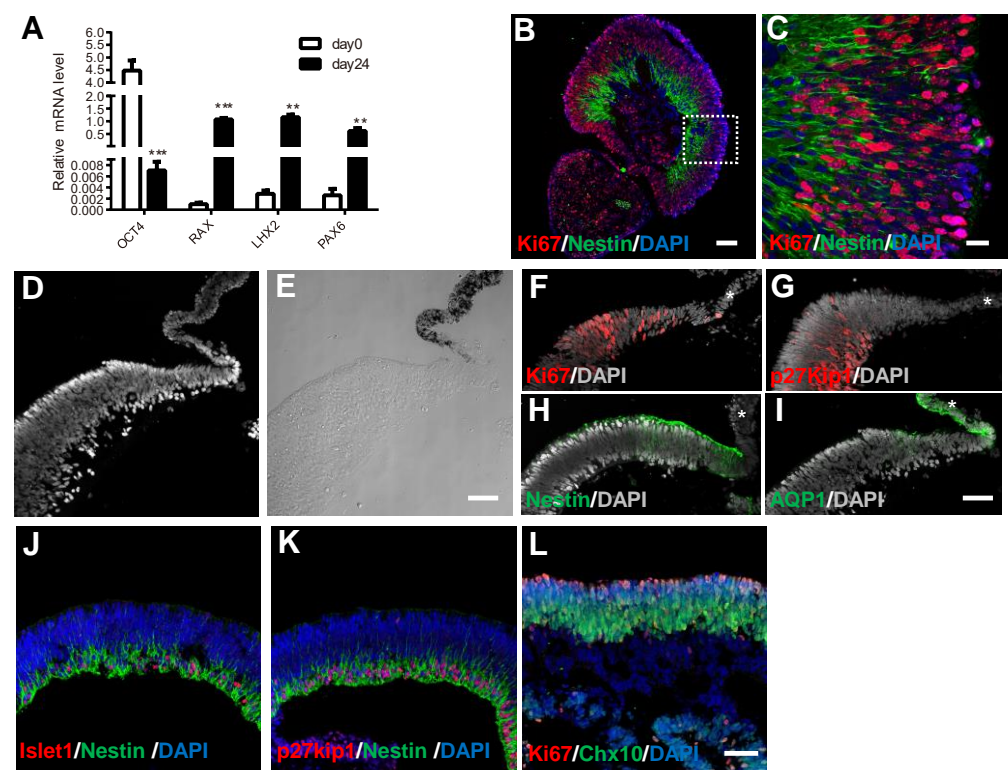
Figure S1. Identification and characteristics of the retinal organoid and CMZ. (A) RT-PCR analysis of mRNA of OCT4, Rax, LHX, and Pax6 in the 3D retinal organoid at D0 and D24. The pluripotent marker OCT4 was robustly downregulated after retinal differentiation while the eye field transcription factors Rax, LHX2, and Pax6 were dramatically upregulated after the formation of the 3D OC. (Mean±SD; D0, n=9; D24, n=9, 3 independent experiments) **p < 0.01; ***p < 0.005. **(B,C)** Immunostaining of 3D human retinal organoids at D24 for Nestin and Ki67. **(D,E)** DAPI staining and a differential interference contrast (DIC) image of the CMZ showing the specific cell shape and arrangement in the CMZ. **(F~I)** Immunostaining of the CMZ at D30 for Ki67 (F), P27kip1 (G), SSEA1 (H), and AQP1 (I). **(J)** Immunostaining of Islet1 and Nestin shows the Islet1^{+} ganglion progenitor cells were colocalized with Nestin at D24. **(K)** Nestin is expressed in the cell body of inner cell layer at D24 in which the CDK inhibitor p27Kip1 is present. **(L)** Ki67+ was distubuted at the most apical layer of the uncommitted Chx10+ retinal progenitor cells. Scale bars: 20 μm (C); 50 μm (D~I), 100 μm (B, J~L).
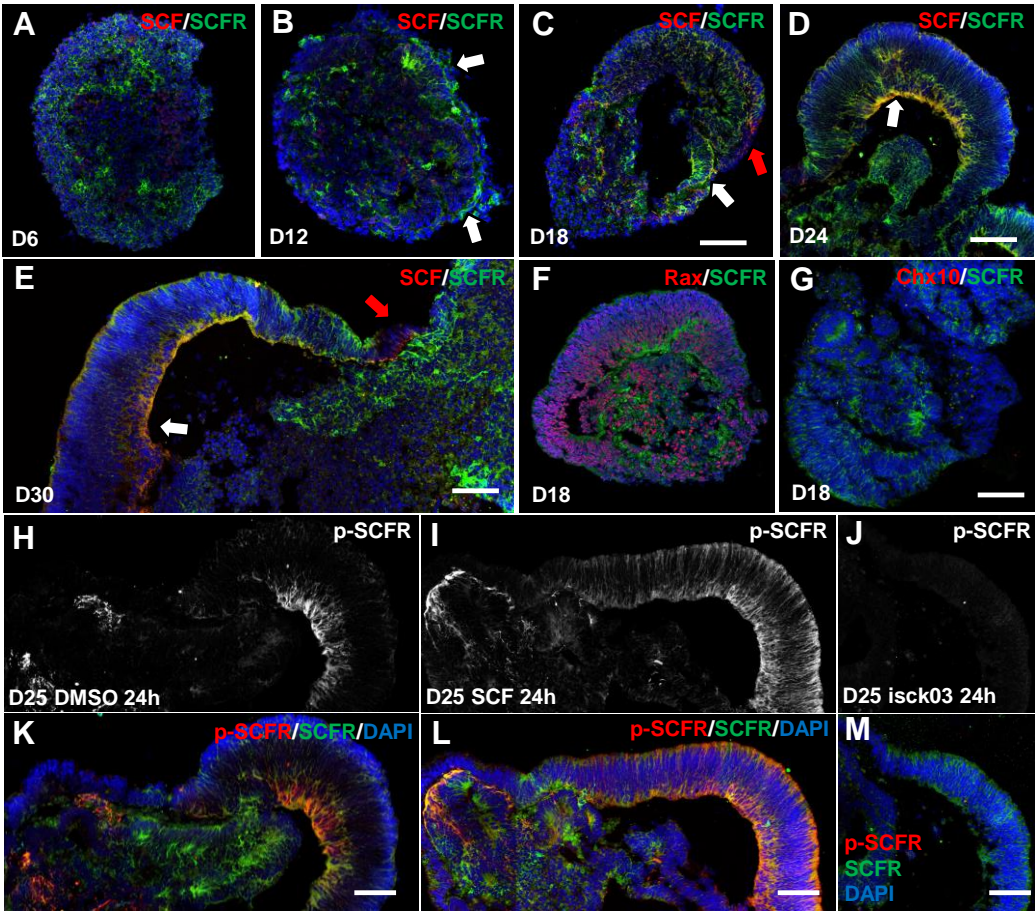
Figure S2. Spatiotemporal expression pattern of SCF and SCFR during the development of retinal organoid and activation of SCF/SCFR signaling pathway.
(A~E) SCFR first emerged at the outer portion of embryonic body at D6(A), gradually enriched at the epithelium-like tissue and cells at D12(B, white arrow), robustly located at the optic vesicle and neural retina at D18 and D24(C, D, white arrow), and preferentially maintained highly expressed in the CMZ and negatively expressed in the RPE at D30(E, white arrow). SCF was not expressed until D18 when the original optic vesicle formed(A~C, red arrow). Location of SCF mainly included two domain: basal side of the central SCFR positive NR and SCFR negative tissue(RPE), meanwhile hardly expressed in the CMZ(D, E, red arrow). **(F~G)** The Rax+ optic vesicle was first emerged at D18 when the neural retina marker Chx10 was not expressed yet. **(H~M)** p-SCFR signal robustly emerged in the basal side of the central NR at D25(H, K); p-SCFR was enhanced by SCF(I, L)and inhibit by isck03(J, M) Scale bars: 100 μm (A~D, F, G); 200 μm (E, H~M).
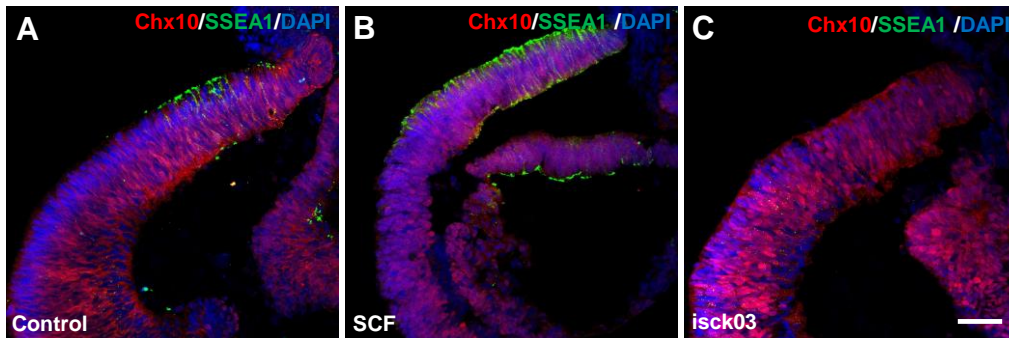
Figure S3. The border of CMZ and NR delimitated by the staining of SSEA1 and Chx10. (A~C) Double-staining of SSEA1 and Chx10 in the control (A), SCF (B), and isck03 (C) treatment group at D30. Scale bars: 100 μm (A~C)
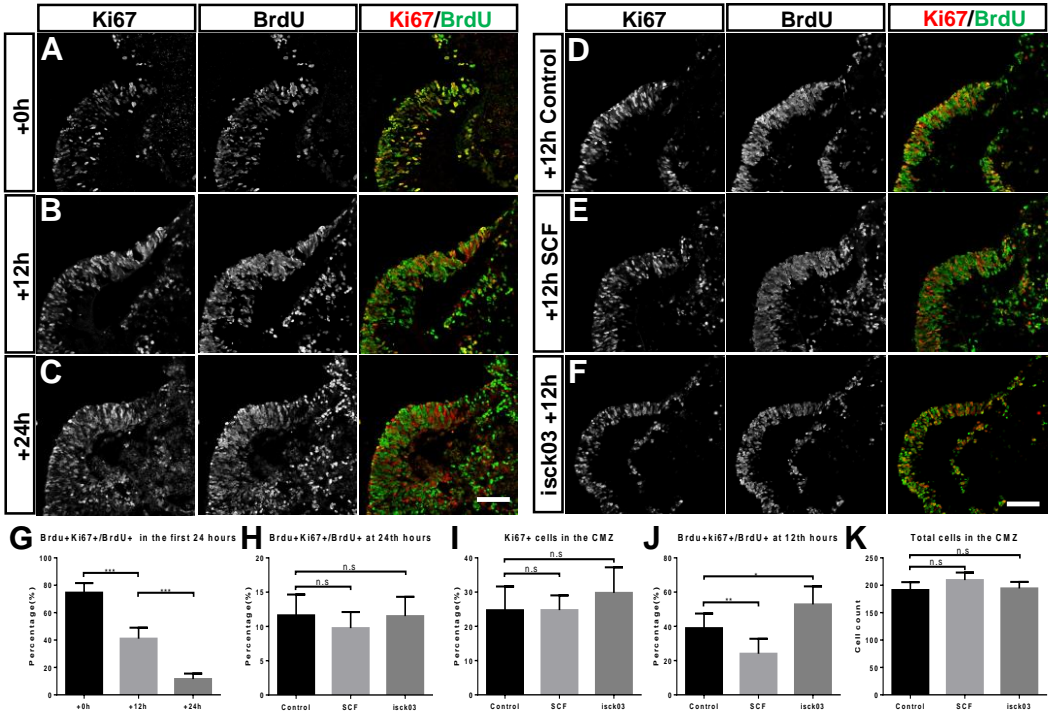
Figure S4. The SCF/SCFR signaling regulated the cell cycle progression of RPCs in the CMZ. **(A~C)** Double staining of BrdU and Ki67 at 0th, 12th, 24th hours after 24 hours BrdU incorporation. **(D~F)** Double staining of BrdU and Ki67 at an intermediate stage of cell cycle(12th hours after 24 hours BrdU incorporation) in the control, SCF, and isck03 treatment group. **(G)** The percentage of BrdU$^+$/Ki67$^+$ cells in the BrdU$^+$ cells at different stage in the first 24 hours after BrdU incorporation. **(H)** The percentage of BrdU$^+$/Ki67$^+$ cells in the BrdU$^+$ cells at the 24th hours after BrdU incorporation. **(I)** The percentage of Ki67$^+$ cells in the total cells of CMZ after 24 hours of SCF or isck03 treatment. **(J)** The percentage of BrdU$^+$/Ki67$^+$ cells in the BrdU$^+$ cells at the 12th hours after BrdU incorporation. **(K)** The cell count of all the cells in the CMZ at D30 after SCF or isck03 treatment. Data are shown as mean±SEM. Independent sample t test.
*p < 0.05, **p < 0.01; ***p < 0.005, ****p < 0.0001. Scale bars: 200 μm (A~F).
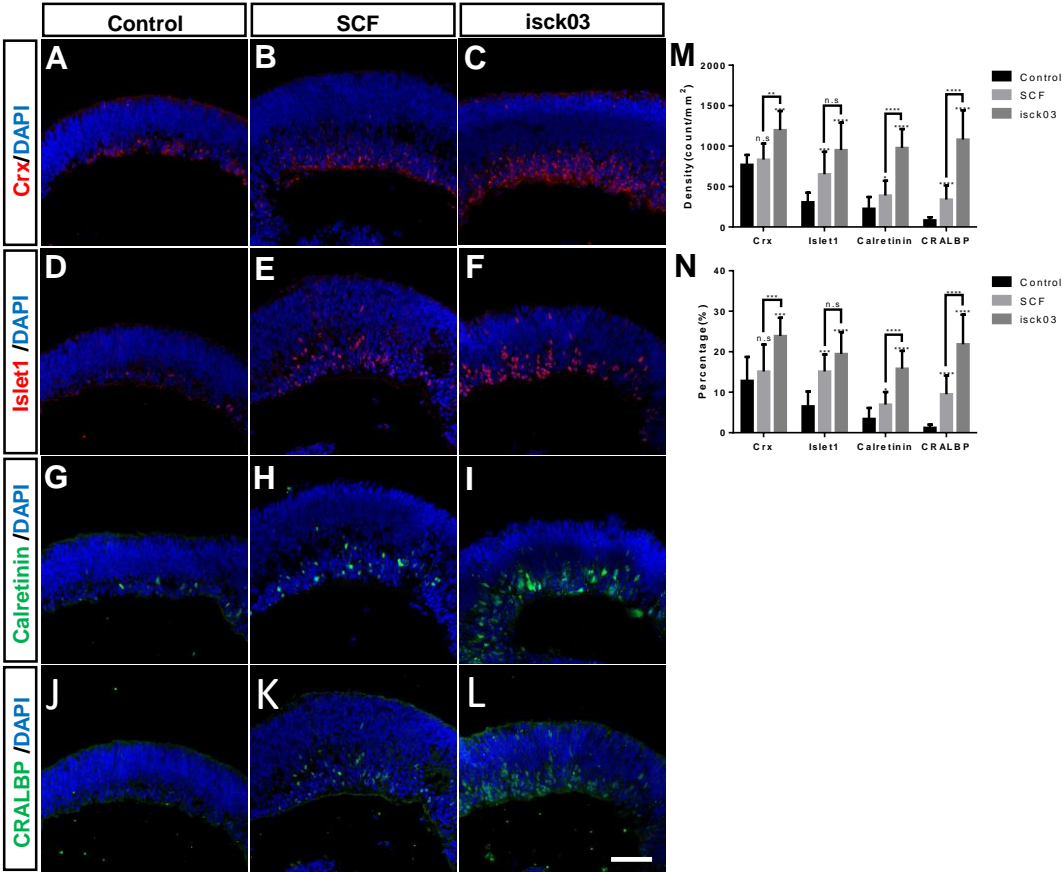
Figure S5. Imbalance of the SCF/SCFR signaling disturbed the early neurogenesis of NR.
(A~L) Immunostaining of each cell type progenitor marker in the control, SCF, and isck03
group at D30: Crx (A~C, red), Islet1 (D~F, red), Calretinin (G~I, green), CRALBP (J~L, green).
M~N, Statistics analysis of cell density and cell percent of each committed progenitor cells
among the control, SCF, and isck03 group. Data are shown as mean±SD. Independent sample
t test. *p < 0.05, **p < 0.01; ***p < 0.005, ****p < 0.0001. Scale bars: 100 µm (A~L).
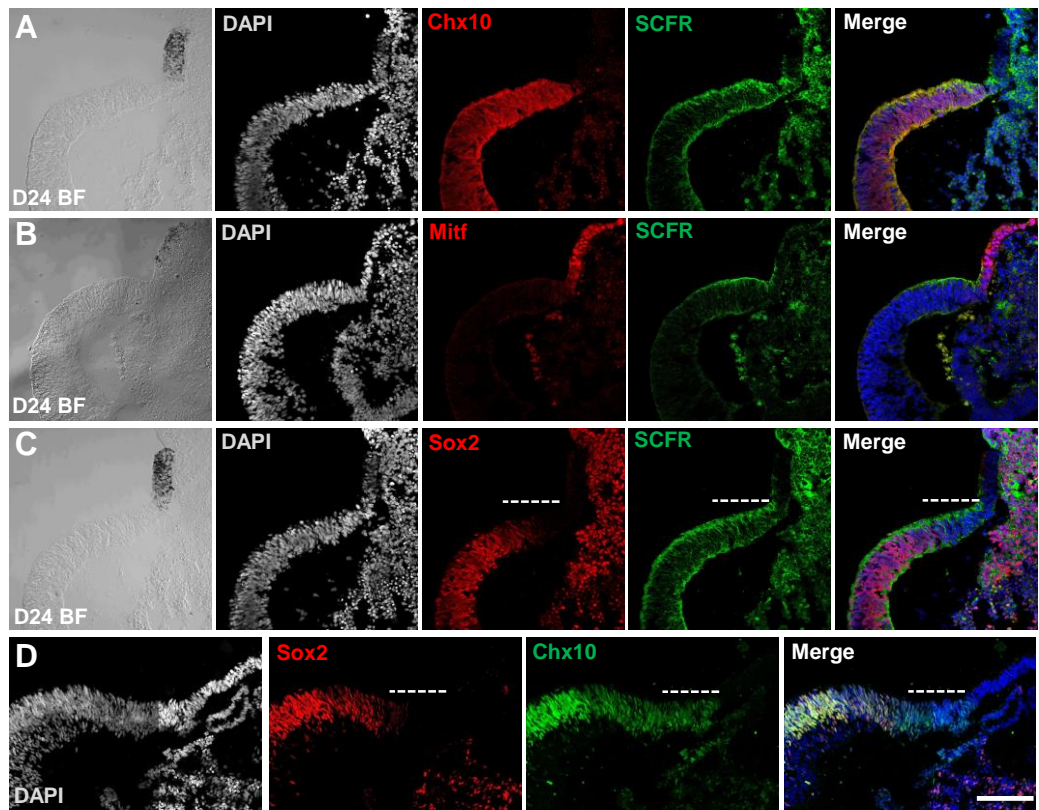
Figure S6. The heterogeneity of cells in the CMZ of human OC.
(A~C) Immunostaining of D24 retinal organoid shows overlapped distribution of SCFR and Chx10(A); distinctive distribution of SCFR and MITF(B); similar distribution of SCFR and Sox2(C). **(D)** Double staining of Chx10 and Sox2 at D24 shows the cell heterogeneity in the CMZ(dashed line: Chx10$^+$Sox2$^-$ region). Scale bars: 200 μm(A~D).